AD-A079 662 CAMBRIDGE UNIV (ENGLAND) DEPT OF ENGINEERING F/G 11/4
MICROMECHANISMS OF FRACTURE OF FIBROUS COMPOSITES IN MONOTONIC --ETC(U)
1979 P W BEAUMONT, P D ANSTICE AFOSR-78-3644
UNCLASSIFIED CUED/C-MATS/TR.54-1979 AFOSR-TR-79-1314 NL

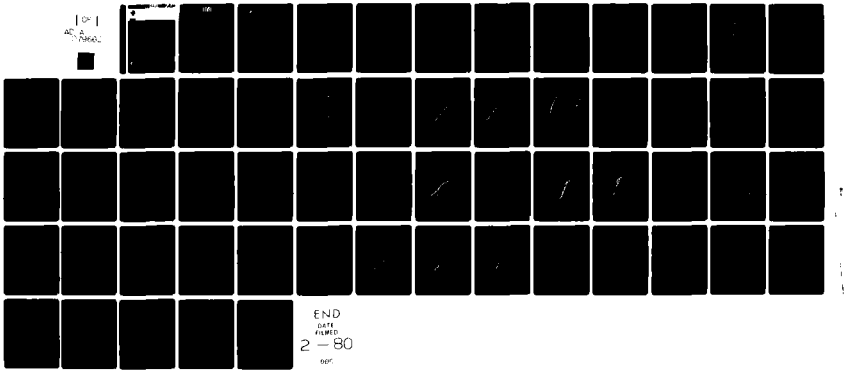

END
DATE FILMED
2 — 80
DDC

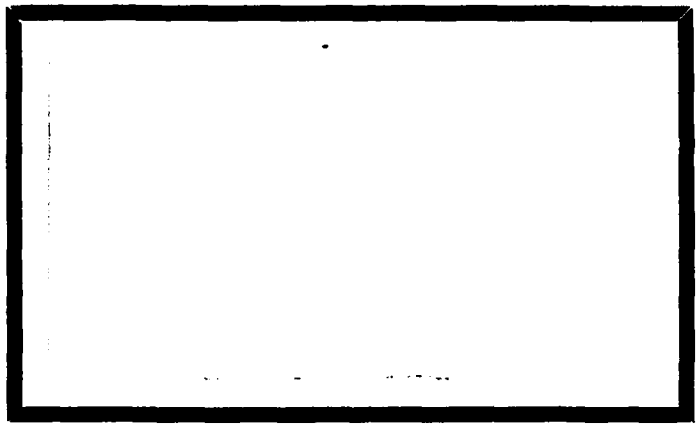

Department of Engineering

LEVEL II

12

MICROMECHANISMS OF FRACTURE OF FIBROUS COMPOSITES IN MONOTONIC LOADING

P.W.R. Beaumont and P.D. Anstice

CUED/C/MATS/TR.54 (1979)

U.S. AIR FORCE EUROPEAN OFFICE OF AEROSPACE (R & D)
London, England

AIR FORCE OFFICE OF SCIENTIFIC RESEARCH
Washington, D.C., U.S.A.

GRANT NUMBER AFOSR-78-3644

UNCLASSIFIED
SECURITY CLASSIFICATION OF THIS PAGE (When Data Entered)

REPORT DOCUMENTATION PAGE	READ INSTRUCTIONS BEFORE COMPLETING FORM
1. REPORT NUMBER: AFOSR-TR-79-1314	2. GOVT ACCESSION NO. / 3. RECIPIENT'S CATALOG NUMBER
4. TITLE (and Subtitle): MICROMECHANISMS OF FRACTURE OF FIBROUS COMPOSITES IN MONOTONIC LOADING.	5. TYPE OF REPORT & PERIOD COVERED: INTERIM rept. 1 Aug 78 – 31 Jul 79
	6. PERFORMING ORG. REPORT NUMBER: CUED/C-MAT/TR 54-1979
7. AUTHOR(s): PETER W R BEAUMONT, PAUL D ANSTICE	8. CONTRACT OR GRANT NUMBER(s): AFOSR-78-3644
9. PERFORMING ORGANIZATION NAME AND ADDRESS: THE UNIVERSITY OF CAMBRIDGE, DEPARTMENT OF ENGINEERING/TRUMPINGTON ST, CAMBRIDGE CB2 1PZ ENGLAND	10. PROGRAM ELEMENT, PROJECT, TASK AREA & WORK UNIT NUMBERS: 2307B2, 61102F
11. CONTROLLING OFFICE NAME AND ADDRESS: AIR FORCE OF SCIENTIFIC RESEARCH/NA, BLDG 410, BOLLING AIR FORCE BASE, D C 20332	12. REPORT DATE: 1979
	13. NUMBER OF PAGES: 57
14. MONITORING AGENCY NAME & ADDRESS (if different from Controlling Office)	15. SECURITY CLASS. (of this report): UNCLASSIFIED
	15a. DECLASSIFICATION/DOWNGRADING SCHEDULE

16. DISTRIBUTION STATEMENT (of this Report)

Approved for public release; distribution unlimited.

17. DISTRIBUTION STATEMENT (of the abstract entered in Block 20, if different from Report)

18. SUPPLEMENTARY NOTES

19. KEY WORDS (Continue on reverse side if necessary and identify by block number)

MICROMECHANISMS
FRACTURE
GLASS FIBERS
CARBON FIBERS
HYBRID
FRACTURE ENERGY

400081

20. ABSTRACT (Continue on reverse side if necessary and identify by block number)

Carbon fibers and glass fibers in brittle matrics fracture by a number of distinguishable mechanisms, matrix cracking, failure of the fiber-matiix bond, fiber fracture, fiber pull-out, and so forth. A large amount of data of fiber debond length and fiber pull-out length have been collected and summarized in cumulative probability diagrams which show the distribution of extreme values. Models of fracture, together with the fracture data are used to construct fracture energy diagrams which show the origins of toughness and the dominate mechanism of

DD FORM 1 JAN 73 1473 EDITION OF 1 NOV 65 IS OBSOLETE

UNCLASSIFIED

failure. Failure analyses have been carried out on glass fibers and carbon fibers in epoxy and polyester resins, and on hybrid composites. Certain generalisations about fracture behavior can be drawn from comparisons of the cumulative probability and fracture energy diagrams.

ABSTRACT

Carbon fibers and glass fibers in brittle matrices fracture by a number of distinguishable mechanisms, matrix cracking, failure of the fiber-matrix bond, fiber fracture, fiber pull-out, and so forth. A large amount of data of fiber debond length and fiber pull-out length have been collected and summarized in cumulative probability diagrams which show the distribution of extreme values. Models of fracture, together with the fracture data are used to construct fracture energy diagrams which show the origins of toughness and the dominant mechanism of failure. Failure analyses have been carried out on glass fibers and carbon fibers in epoxy and polyester resins, and on hybrid composites. Certain generalisations about fracture behaviour can be drawn from comparisons of the cumulative probability and fracture energy diagrams.

INTRODUCTION

There exists a number of distinguishable mechanisms by which a fibrous composite can fail; by matrix cracking; by fiber-matrix debonding, by fiber fracture, by fiber pull-out and so forth (Fig. 1). Models to describe failure processes like these can be derived; they are based on direct microscopic observation of fibers debonding, snapping and pulling out of cracked matrices. Three mechanisms will be described by which a fibrous composite can fail, using a sequence in which they may occur. An equation will be selected for each mechanism, based on a physically sound microscopic model, to describe quantitatively each failure process. A large amount of fracture data for glass fibers and carbon fibers in polyester, epoxy, and hybrid composites will be presented in cumulative probability diagrams. These diagrams are based on fractographic information on fiber-matrix debonding and fiber pull-out processes and show the probability of a fiber debonding over a particular distance and pulling out over a certain length during composite fracture. Each failure model is then used in turn, together with the failure data to estimate the energy dissipated by the various fracture mechanisms during crack propagation. The energy data are displayed in fracture energy diagrams which show fracture energy as a function of the number of fibers, or in the case of the hybrid composite, proportion of the two kinds of fiber. Comparison is then made between theory and experimental work of fracture data, and between diagrams, and the dominant mechanism of failure is apparent. Certain generalisations about fracture behaviour between materials can be drawn. Each mechanism will undoubtedly depend, in its own way on environment, temperature and humidity, for example; at this time, attention is paid to fracture under ambient conditions, although comment is made on an aging effect.

An important point to remember is that when moving from one composite system to another, the dominant mechanism of fracture may change. Another point worth emphasizing is that the sequence of microscopic failure events can vary from one composite to another, and the energies dissipated, and their origins, can be quite different in the crack initiation and crack propagation stages of fracture.

The properties of glass fibers, carbon fibers and a typical polyester or epoxy resin are listed in Table 1.

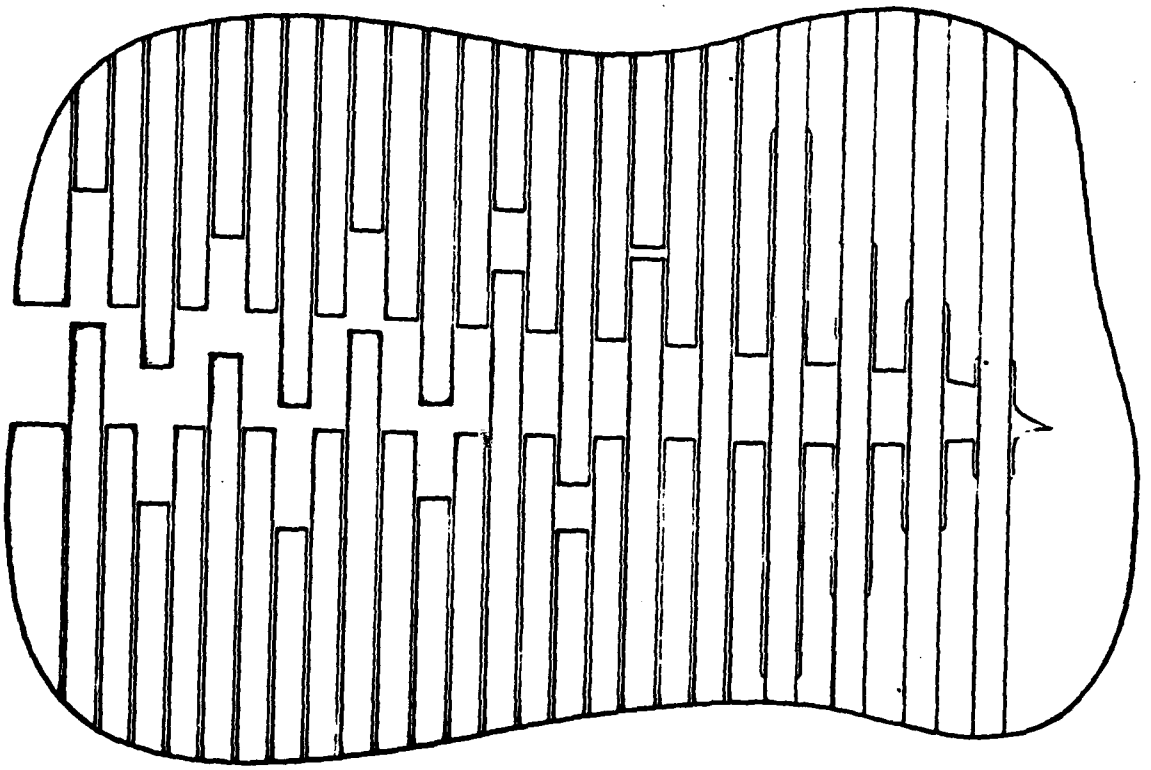

Fig. 1 Schematic representation of various modes of failure in a brittle fibrous composite in the vicinity of a crack front.

TABLE I

Fiber and matrix properties

Material	No. of fibers per tow	Fiber diameter (10^{-6} m)	Tensile strength (GN m^{-2})	Young's modulus (GN m^{-2})	Failure strain ε
Carbon fiber Type II	5000	8	2.40	240	0.010
Glass Fiber Type E	1600	13	1.65	70	0.023
Typical Epoxy Resin or Polyester Resin	-	-	0.06	2.5	0.014

MODELLING MICROMECHANISMS OF FRACTURE

Consider the propagation of a crack in a brittle matrix, around and beyond a long, strong fiber, glass fiber in polyester, for instance, (Fig. 2). Localised stresses at the tip of the crack are likely to cause a breakdown of the fiber-matrix bond. Under conditions of increasing load, the crack faces of the matrix separate and the interfacial debonded region, on either side of the matrix crack, extends. Relative displacement between fiber and matrix can then occur over the entire length of debonded fiber. Provided the fiber still interacts in some way with the matrix, by mechanical keying at the interface, for instance, a frictional (sliding) shear force is established soon after the bond fails. The distance over which this shear force acts is approximately equal to the product of the debonded length of fiber, ℓ_d, and the differential failure strain of fiber and matrix, $\Delta\varepsilon$. Since the initial frictional shear force, $\tau\pi d(\ell_d/2)$, acts in each direction from the fracture surface of the matrix over a distance, $\Delta\varepsilon\ell_d/2$, the work done per fiber is (1, 2)

$$W_{pdf} = \pi d\tau \ell_d^2 \, \Delta\varepsilon \qquad (1)$$

$$= \pi d\tau \ell_d^2 \, \varepsilon_f/2 \qquad (2)$$

provided $\varepsilon_f \gg \varepsilon_m$. This is a reasonable assumption for a brittle matrix which cracks at low strains. (d is the diameter of fiber).

The load on a fiber is a maximum in the debonded region and as it increases the fiber is likely to break at a flaw somewhere along its debonded length (Fig. 3). The localised elastic work of tensile deformation, W_d, in the fiber over a length, ℓ_d, (sometimes referred to as fiber debonding energy (3)), can be expressed as

$$W_d = \pi d^2 \sigma_f^2 \, \ell_d/8E_f \qquad (3)$$

This equation does not account for the recoverable energy as the load builds up in the fiber over a distance $\ell_c/2$ from the point of fiber fracture* (4,5). σ_f and E_f are the tensile strength and Young's modulus of the fiber, respectively.

Provided there is some kind of interaction between the debonded fiber end and matrix, then a frictional (sliding) shear force opposes any applied force to extract the fiber (6), (Fig. 4). The total frictional work of pull-out is

---

* A critical fiber length, ℓ_c, is defined as the smallest length of fiber which, when embedded in a matrix, can be loaded to its breaking point.

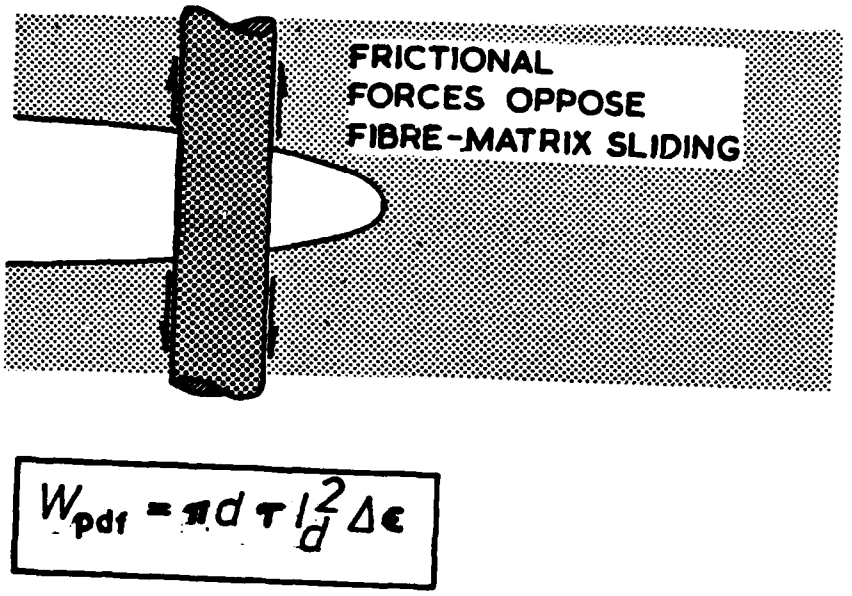

Fig. 2 A loaded fiber debonds and slips in the matrix socket behind an advancing crack front.

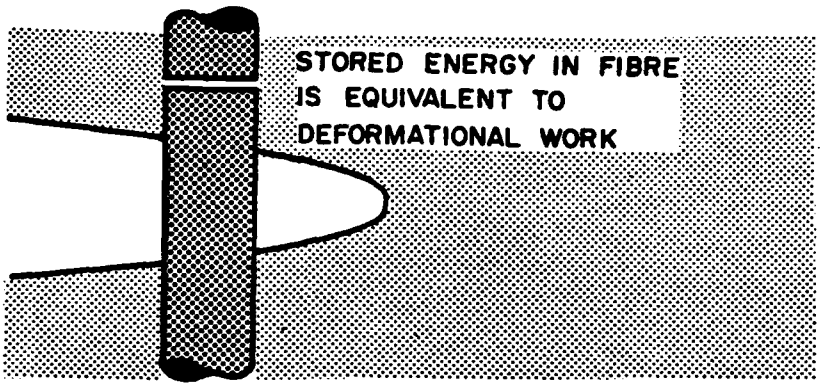

$$W_d = \pi d^2 \sigma_1 l_d^2 / 8 E_1$$

Fig. 3 An overloaded fiber snaps at a weak point in the debonded region of the fiber as the crack front advances.

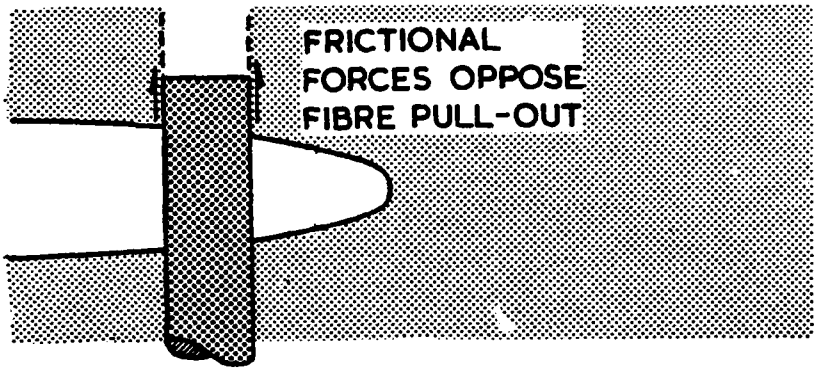

$$W_p = \pi d \tau l_p^2 / 2$$

Fig. 4 A broken fiber pulls out of its matrix socket as the fracture surfaces of the cracked matrix separate.

$$W_p = \pi d\tau \ell_p^2/2 \qquad (4)$$

The average work to extract a fiber whose embedded length lies between 0 and ℓ_p is, therefore,

$$W_p = \pi d\tau \ell_p^2/6 \quad (\ell_p < \ell_c/2) \qquad (5)$$

assuming a constant frictional shear stress, τ.

The frictional shear stress can be estimated using the expression (1)

$$\tau = \sigma_f d/2\ell_c \qquad (6)$$

In a fiber pull-out experiment, the maximum length of fiber that can be extracted from a block of matrix without first breaking is equal to $\ell_c/2$. Equations (2) and (5) can be rewritten, therefore, in terms of ℓ_d and ℓ_p;

$$W_{pdf} = (\pi d^2 \sigma_f \varepsilon_f/8) \quad (\ell_d^2/\ell_p) \qquad (7)$$

$$W_p = \pi d^2 \sigma_f \ell_p/24 \qquad (8)$$

In each model, the work done is directly proportional to the number of fibers and each mechanism, in its own way, is sensitive to the interfacial shear stress. We have assumed that the interfacial shear stress is a constant. This may not be true; the frictional shear stress depends upon the radial force exerted by the matrix onto the fiber which is likely to be sensitive to the spacing between fibers and fiber bundles.

From the above relationships, we can identify three contributions to the total work to fracture the composite. The work to fracture the composite can be written in terms of ℓ_d and ℓ_p;

$$W_T = (\pi d^2/4) \quad [(3\sigma_f \varepsilon_f) \quad (\ell_d^2/\ell_p) + (\sigma_f^2 \ell_d/E_f) + (\sigma_f \ell_p)] \qquad (9)$$

where ℓ_d is the distance over which the fiber has debonded and ℓ_p is the maximum fiber pull-out length.

FAILURE ANALYSIS

Statistical methods

The statistical prediction of failure relies on the characterisation of a flaw strength distribution function. One form of the extreme value distribution is

$$S = \exp (-\sigma/\sigma_o)^m V \qquad (10)$$

where S is the probability of survival, σ is an applied stress on a specimen of volume V, and m and σ_o are the extreme value distribution parameters. The variability of a set of data decreases as m increases;

m and σ_o therefore characterise the material for prediction of structural reliability.

In logarithmic form, equation (10) can be written

$$\ell n\ (-\ell n\ S) = m(\ell n\sigma - \ell n\sigma_o) \qquad (11)$$

m is the gradient of a linear plot of $\ell n\ (-\ell n\ S)$ and $\ell n\ \sigma$, and $\ell = \ell_o$ when $S = e^{-1} = 0.37$.

Each mechanism of failure in a fiber composite is affected by the statistical aspects of fiber-matrix bond strength and the distribution of weak points along the fiber. This is why a broken fiber composite has a variability of lengths of fibers protruding above the fracture surface. A quantitative assessment of failure therefore requires a statistical analysis of the micromechanisms of fracture; fiber pull-out length, for example, is likely to be affected by the distribution of weak flaws along the length of fiber. Equation (10) can be written in terms of the probability of a fiber debonding or pulling out over a particular distance, ℓ,

$$P(\ell) = \exp\ (\ell/\ell_o)^m \quad (V = 1) \qquad (12)$$

The mean value, $\bar{\ell}$, of a distribution of data of the form

$$P(\ell) = f(\ell) \qquad (13)$$

can be expressed as

$$\bar{\ell} = \int_{\ell_1}^{\ell_n} (\ell\ dP/d\ell)\ d\ell \qquad (14)$$

For the case of an extreme value distribution, the mean value, $\bar{\ell}$, can be expressed

$$\bar{\ell} = \int_{\ell_1}^{\ell_n} m(\ell/\ell_o)^m\ \exp\ (-\ (\ell/\ell_o)^m)d\ell \qquad (15)$$

and $\bar{\ell}$ determined from known values of m and ℓ_o.

Cumulative probability diagrams can summarize a considerable amount of fractographic information on fiber-matrix debonding and fiber pull-out. They show a distribution of extreme values of fiber lengths and by presenting the data in logarithmic form (equation 11), values of m and ℓ_o can be determined. These parameters, together with equation (15) are used to determine values of $\bar{\ell}$ for fiber debonding and fiber pull-out.

The procedure is as follows; after fracture, an attempt is made to assign a mode of failure to a group of specimens, based on fractographic observations of fiber debonding and fiber pull-out. Model composites in the form of a prismatic bar of transparent resin containing a layer of unidirectional fiber tape can be used for this purpose. Figure 5 shows such a beam loaded in 3-point bending. In this case, close to the tensile face of the specimen, is a single tow of carbon fibers containing 5,000 individual filaments and two strands of glass fibers on either side, each strand containing 1,600 individual filaments. Bundles of glass fibers and carbon fibers, like these, can be arranged in various ways to produce a series of composites ranging from a glass fiber composite to a carbon fiber composite, with many combinations of glass and carbon fibers between the two extremes, (Fig. 6).

A precise measurement of fiber debond length and fiber pull-out length after composite fracture is important. An optical microscope can be used for this purpose. Tracings are made of each protruding bundle of fibers, carefully following the dark outline of the pulled-out fibers and the fracture plane of the matrix. Similarly, tracings are made of the debonded fiber regions which are clearly visible in reflected light. An average value of the longest fibers extracted from the matrix and an average value for the length of debonded fibers for each bundle of fibers is determined by dividing the area of each tracing by the width of the bundle, (Fig. 7). If there are 5 strands of glass fiber in each specimen in a group of 20 specimens, for example, then 200 tracings are made of protruding fibers and 200 tracings of debonded fibers, since both halves of each specimen can be examined. Values of fiber debond length and fiber pull-out length are tabulated and cumulative probability diagrams constructed. If we assume a normal distribution of pulled out fiber ends between 0 and ℓ_p, then the average length of extracted fiber is $\ell_p/2$.

The work to fracture each composite is determined by integrating the load/displacement relationship obtained in the 3-point bending experiment. For glass fiber and carbon fiber composites, the work of fracture is some 2-3 orders of magnitude greater than the work of fracture of pure resin. We have chosen, therefore, to normalise our work of fracture values with cross-sectional area of the fibers. In this way, comparison between the models of fracture and experiment can be made.

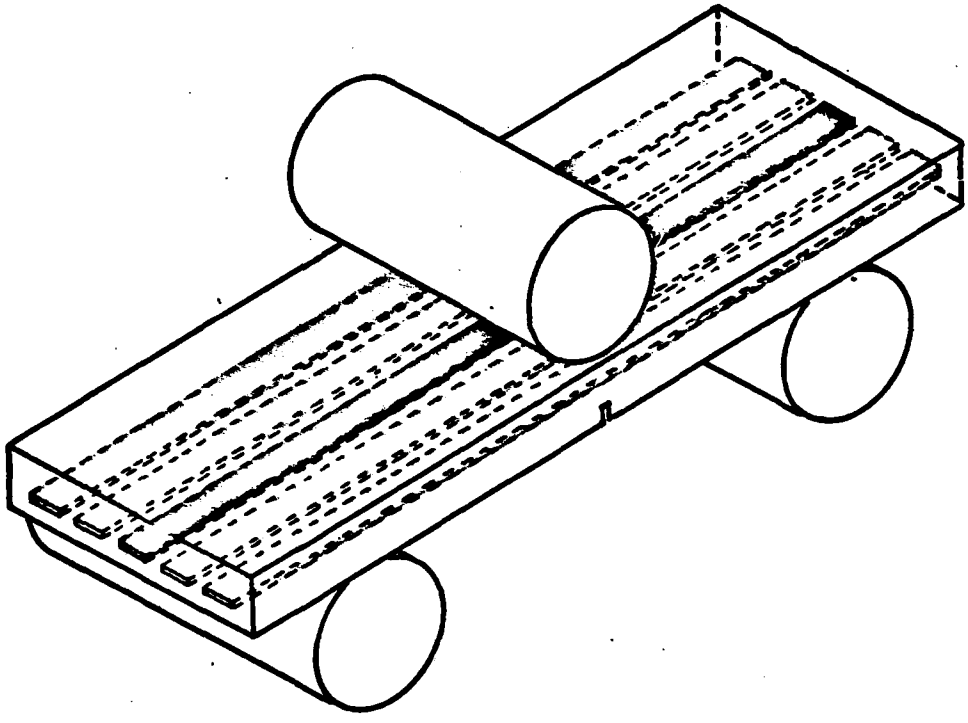

Fig. 5 A bar of transparent resin containing a single layer of unidirectional hybrid tape close to the tensile face in a 3-point bend test. The centre bundle or tow of carbon fibres contains 5000 individual filaments. Two strands or rovings of glass fibers containing 1600 filaments are on either side. (Dimensions of the specimen are 200 mm × 10 mm × 2 mm).

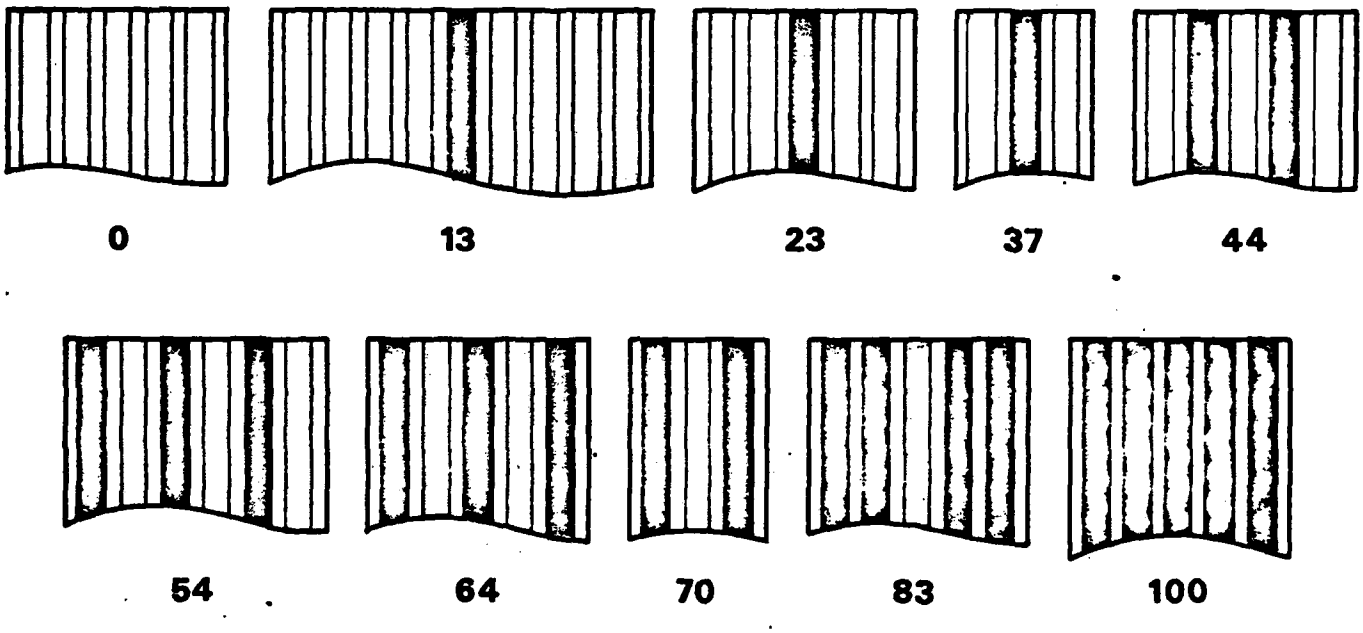

Fig. 6. Various combinations of carbon fiber and glass fiber bundles in unidirectional hybrid tapes used in the manufacture of model specimens.

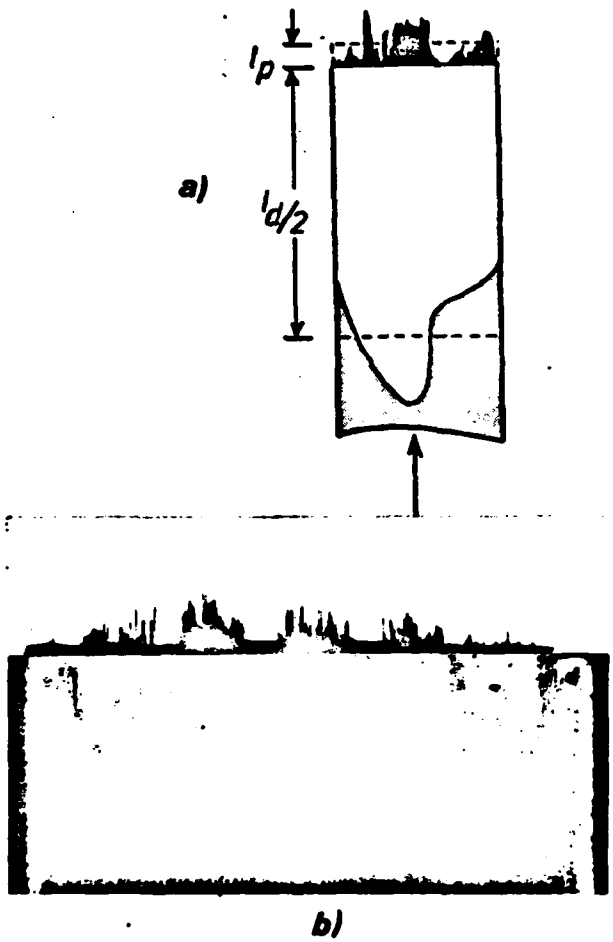

Fig. 7. A photomicrograph (b) of a central tow of carbon fibres with two strands of glass fibers on either side. The broken half of a specimen shows profiles of pulled out fibers (dark regions) and debonded fibers (light regions). The sketch (a) represents the pulled out and debonded fibers of one of the glass fiber strands, defining ℓ_p and ℓ_d.

Glass fibers in epoxy

Figure 8 shows cumulative probability versus fiber debond length, ℓ_d, for different numbers of glass fibers in epoxy. The data does not overlap but are displaced slightly to higher values of ℓ_d as the number of fibers increases. It seems that the debonding process is sensitive to the number of glass fibers in the resin. It is interesting to note, (although it is not obvious why), the data for N = 4800 fibers falls to the right of the data for N = 6400 fibers. This apparent reversal in trend in the shift of cumulative probability data will be referred to later when we discuss fracture energy. A similar shift of data towards higher fiber lengths is observed for pulled out fibers (Fig. 9). The apparent oddity in this case is the disproportionate displacement of data for N = 8000 fibers. Metallographic examination of various specimens showed excellent penetration of the fibers with resin and the idea that poor wetting of the fibers is responsible for the movement of data to higher values is not correct.

The extreme value distribution equation can describe each set of data. The parameters m and ℓ_o which appear in equation (12) and later in equation (15) are determined by replotting the data in logarithmic form, (Fig.10). Presenting data in this way is useful for characterising modes of failure and for observing the subtle effects of environment, moisture for instance. Later in this section, we show the effect of aging on the distribution of extreme values of fiber debonding and fiber pull-out.

Combining equation (15) with values of m and ℓ_o enables us to determine the mean length of debonded and pulled out fibers. Table II lists values of m, ℓ_o and $\bar{\ell}$ for the debonding and pulling out of glass fibers in epoxy. For comparison, values of the arithmetic mean of fiber debond length and fiber pull-out length are shown alongside $\bar{\ell}$ calculated using equation (15).

In view of the agreement between the two methods of determining $\bar{\ell}$, the arithmetic means of fiber debond length and fiber pull-out lengths, together with the expressions of fracture energy, are used to estimate the energy of each mechanism of failure and total theoretical fracture energy of the composite. A diagram of fracture energy versus number of glass fibers (Fig.11) shows the estimated energy dissipated during

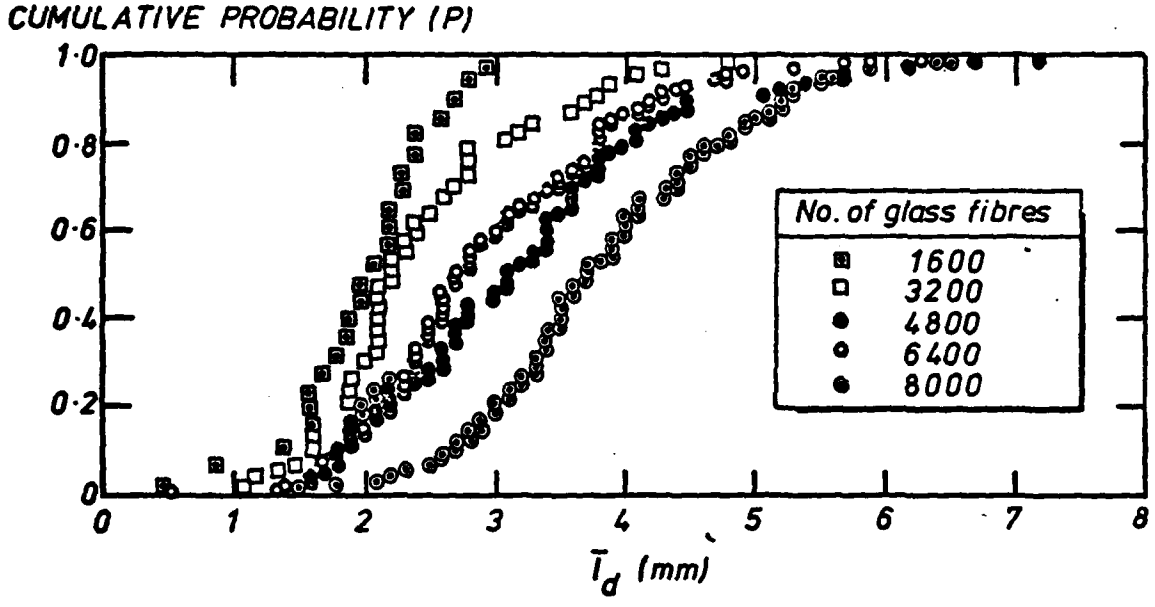

Fig. 8 Extreme value distributions of lengths of debonded glass fibers in epoxy for different numbers of strands in the model specimens. (1 strand contains 1600 filaments, 2 strands contains 3200 filaments, and so forth.)

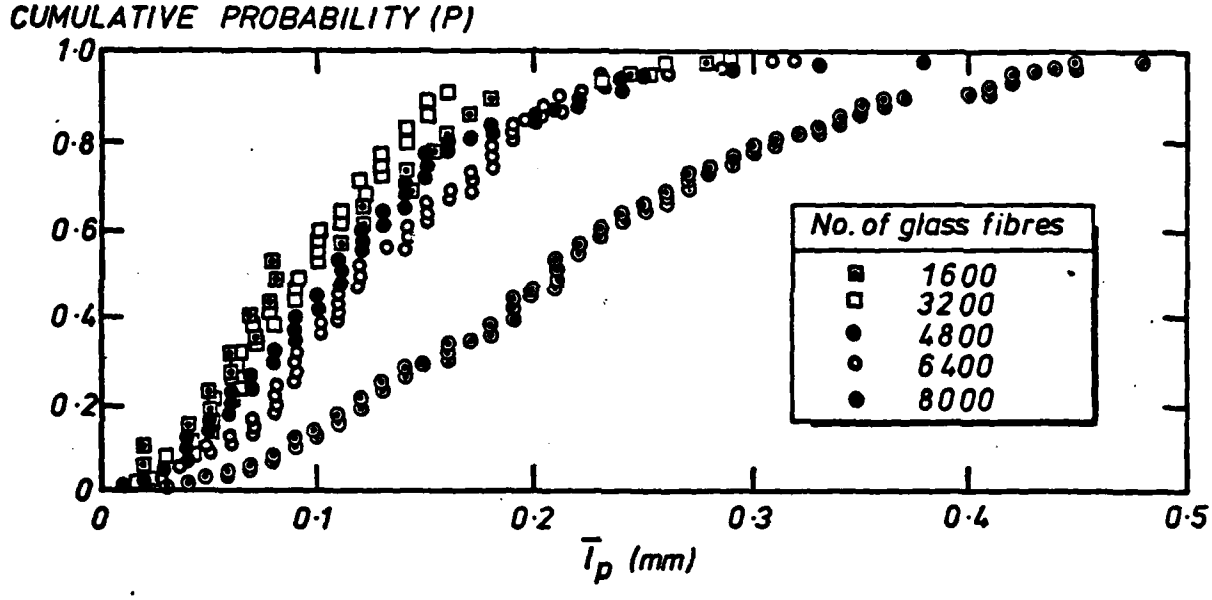

Fig. 9 Extreme value distributions of lengths of pulled out glass fibers in epoxy obtained from measurements made on the specimens used to construct Fig. 8.

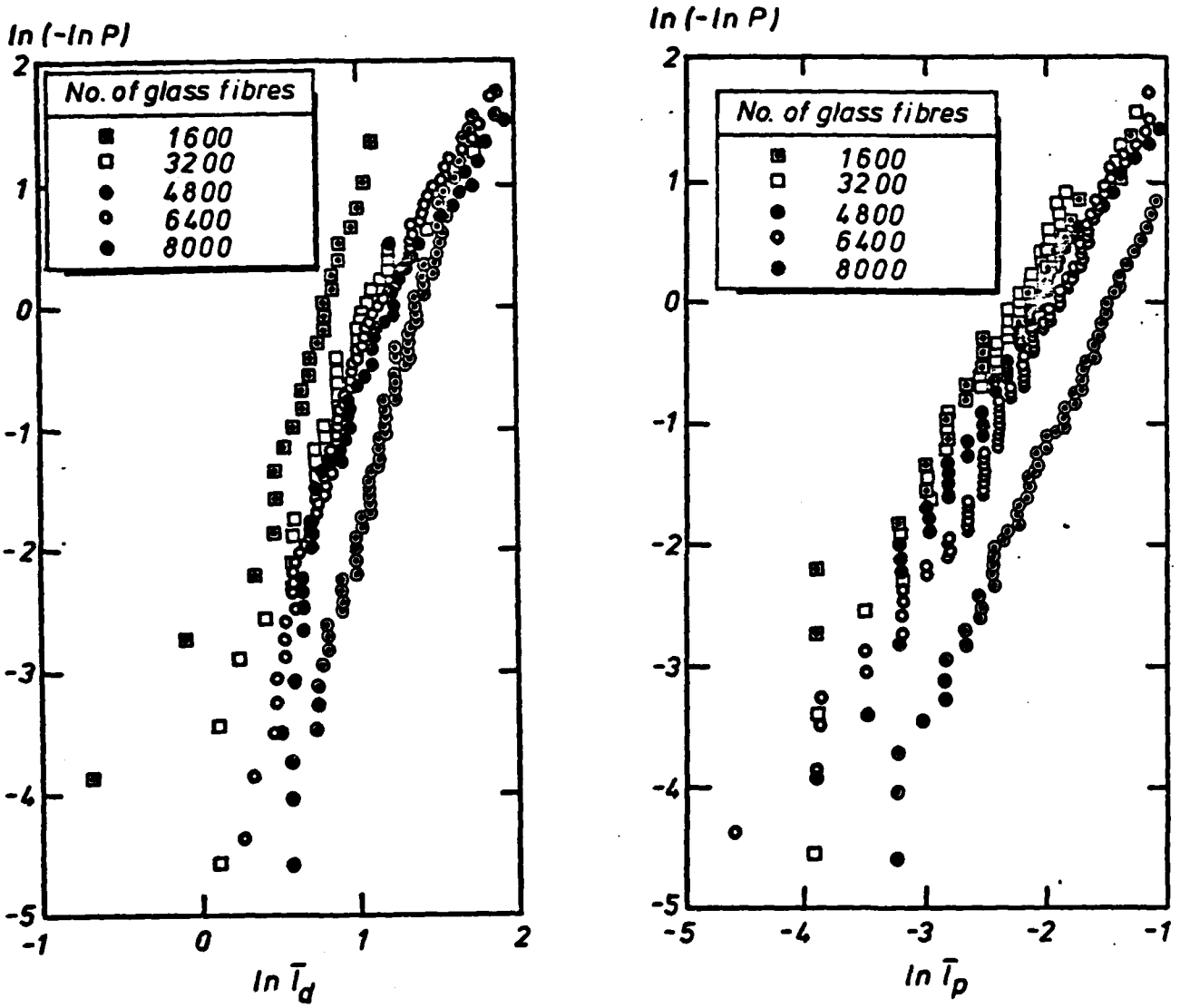

Fig. 10 Logarithmic plots of the data presented in Figs. 8 and 9.

TABLE II

A summary of values of m, ℓ_o and $\bar{\ell}$ for glass fibers in epoxy

No. of glass fiber rovings	Fiber debond length (mm)				Fiber pull-out length (mm)			
	m	ℓ_o	$\bar{\ell}$(eq. 15)	$\bar{\ell}$(arithmetic)	m	ℓ_o	$\bar{\ell}$(eq. 15)	$\bar{\ell}$(arithmetic)
1	3.1	2.3	1.7	2.0	1.5	0.12	0.09	0.11
2	3.6	2.7	2.4	2.5	2.0	0.11	0.10	0.11
3	3.1	3.6	3.2	3.2	1.9	0.14	0.13	0.13
4	3.5	3.3	3.0	3.0	1.9	0.15	0.13	0.13
5	4.6	4.2	3.8	3.9	2.2	0.25	0.22	0.24

the post-debond fiber sliding mechanism (equation 7). The relationship is not a simple linear one as one would expect from the form of the equation; the cumulative probability data showed fiber debond length to be sensitive to the number of fibers in the composite. We recall that it is the square of the fiber debond length and number of fibers which appears in the post-debond fiber sliding equation. The plateau to the curve reflects the reversal in the trend in shift of cumulative probability data for N = 6400 fibers to which reference was made earlier.

An estimation of the fiber debond energy (equation 3) is shown in the next diagram (Fig.12). At first sight, the shape is linear but closer examination shows a smooth curve with a gradually increasing slope. It reflects the dependence of fiber debond length on the number of glass fiber strands. The plateau shown in the previous figure is less obvious since fiber debond energy is directly proportional to the length of debonded fiber. The energy dissipated in this way is significantly less than the work done in the post-debond fiber sliding mechanism.

The work to pull broken glass fibers out of a cracked matrix (equation 8) is of a similar order of magnitude as the fiber debond energy (Fig.13). Both figures have a similar shape; the increase in gradient of the curve at the high numbers of fibers originates from the high values of fiber pull-out length shown previously in the cumulative probability data for N=8000 fibers.

The result of summing these 3 energy parameters (equation 9) is shown in Figure 14. Apart from a small rise in the curve at N=5000 fibers, approximately, it is a smooth curve with a gradually increasing slope as the number of fibers increases. Comparison of the empirical diagram with experimental work of fracture data shows remarkable likeness in shape and magnitude (Fig. 15). From observations of the fracture of glass fibers in epoxy we know that the composite exhibits all the common modes of failure; matrix cracking, fibers debonding, fibers snapping and fibers pulling out. The dominant toughening mechanism appears to be post-debond sliding between fiber and matrix; the breakage of fibers and the pulling out of the broken fiber ends dissipates similar amounts of energy and together contribute little more than one-quarter of the total fracture energy of the composite.

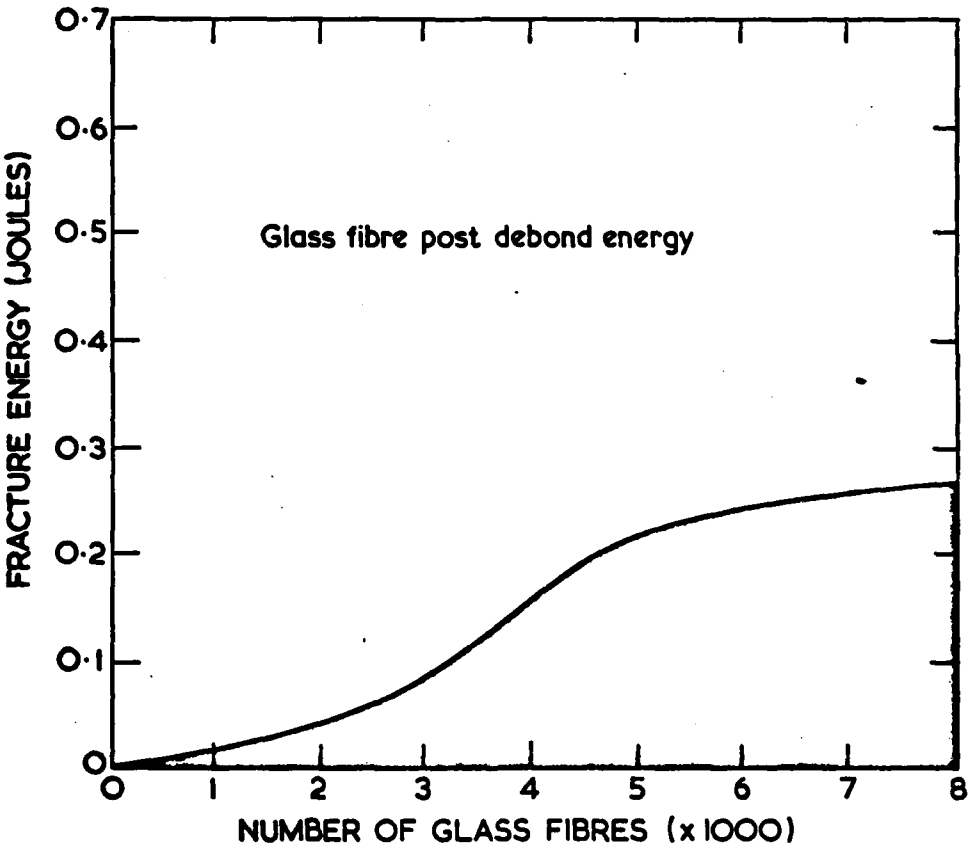

Fig. 11. An estimation of the energy dissipated during post-debond sliding of glass fibers in their epoxy matrix sockets, based on data of fiber debond length and fiber pull-out length, together with eq. (7).

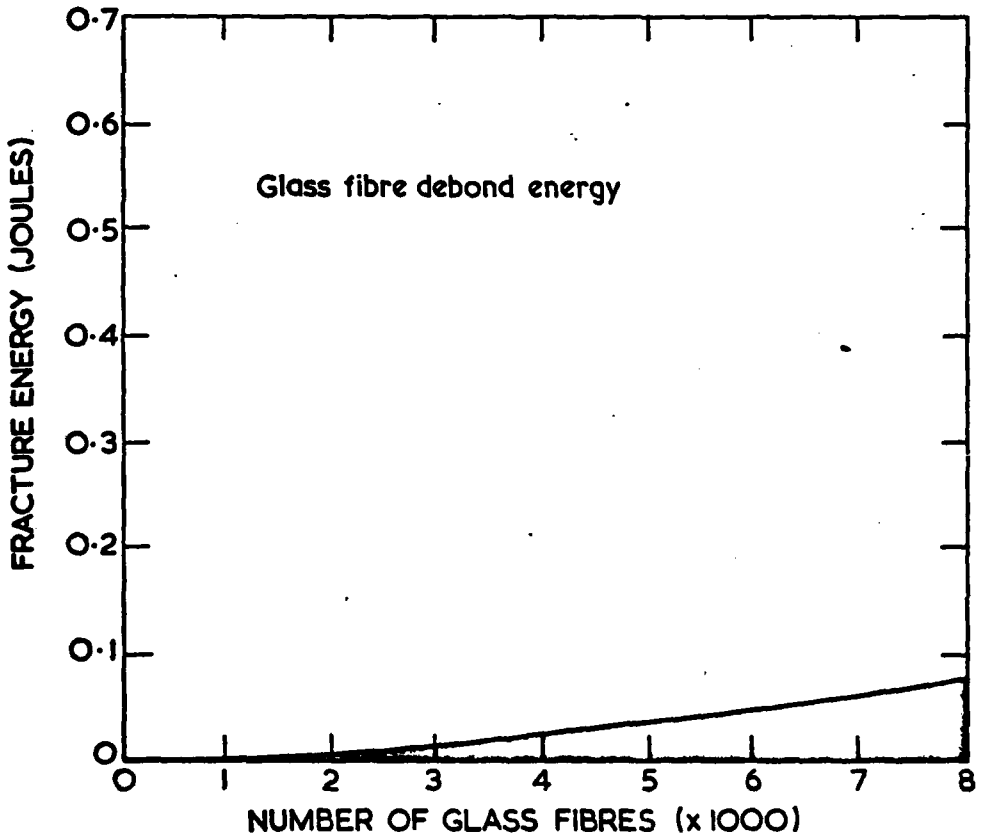

Fig. 12 An estimation of the release of stored elastic strain energy when a debonded glass fiber snaps, based on data of fiber debond length, together with eq. (3).

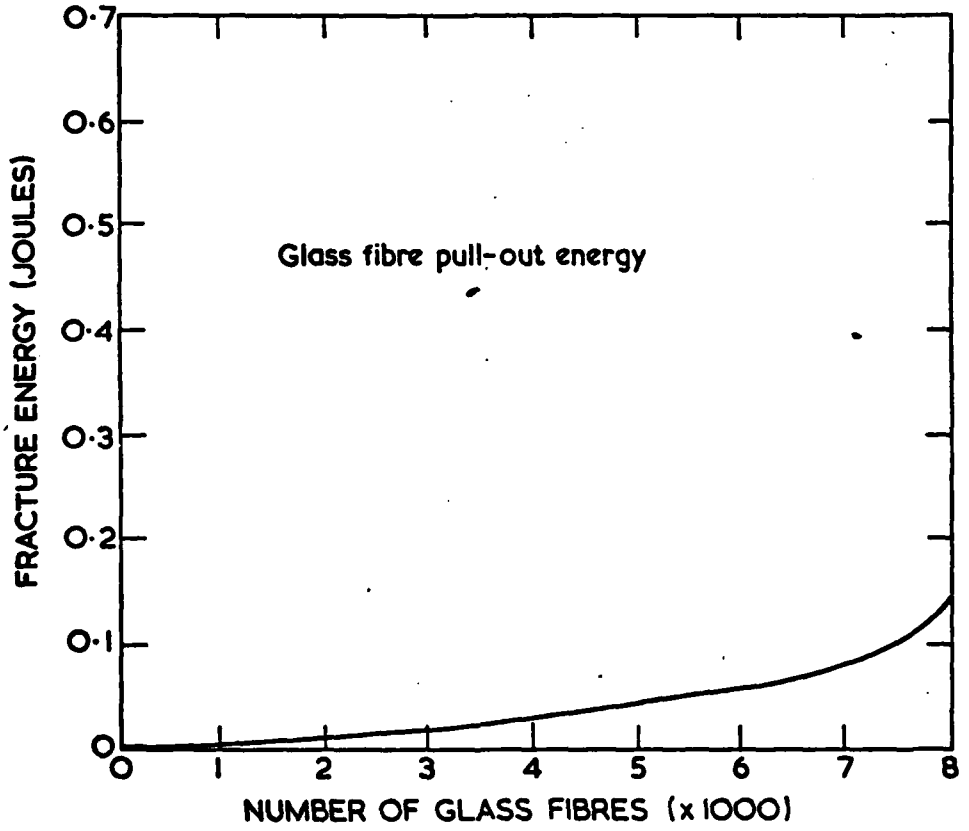

Fig. 13 An estimation of the work done in pulling broken glass fibers out of their epoxy matrix sockets, based on data of fiber pull-out length, together with eq. (3).

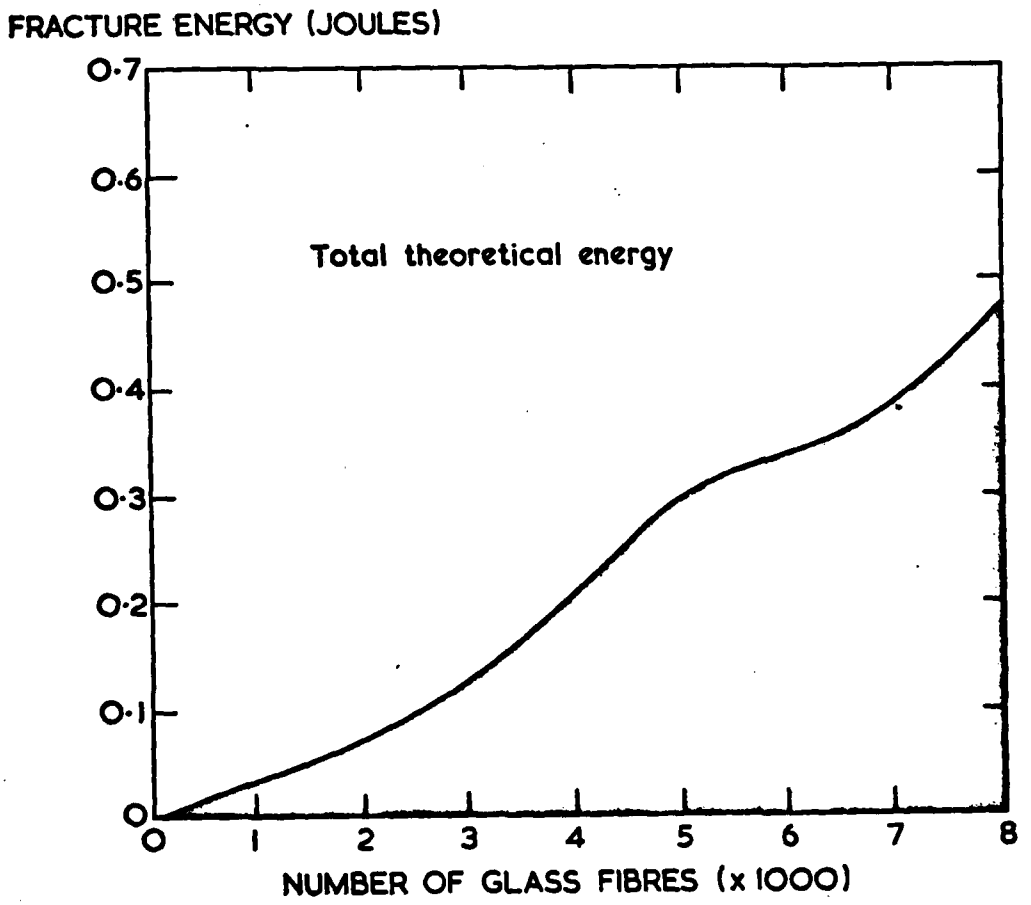

Fig. 14 Total theoretical fracture energy of glass fibers in epoxy determined by combining data of fiber debond length and fiber pull-out length with eq. (9).

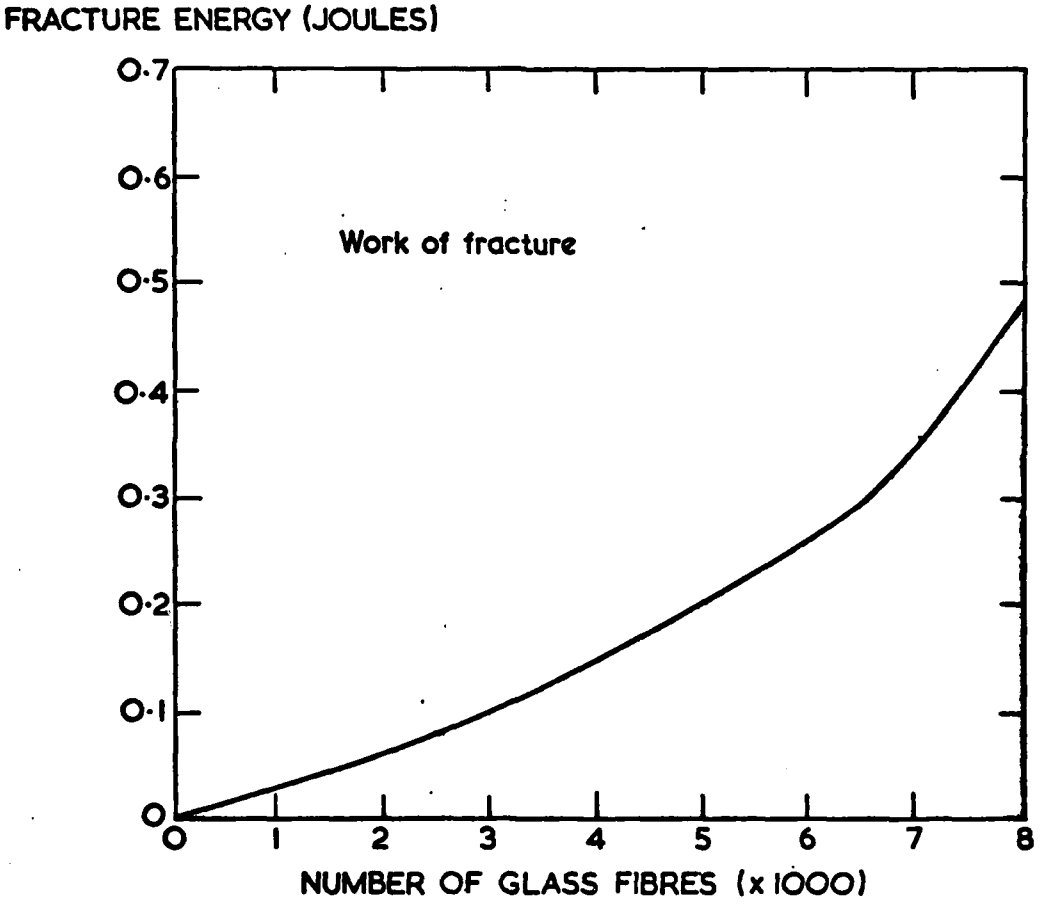

Fig. 15 Experimental work of fracture for glass fibres in epoxy.

Aging effects on toughness

Some of the glass fiber-epoxy specimens were stored at 18 (±2) °C, 65 % R. H. for 6 months before testing. The distances over which the fibers debonded and pulled out are shown in cumulative probability diagrams (Figs. 16, 17). In one case, aging of the composite has resulted in the data being displaced to lower values of debonding. The inference is that the aging process, (by whatever means), has increased the strength of the glass fiber-epoxy bond with a corresponding decrease in the distance over which the fiber debonds. It may be that additional curing and cross-linking of the resin with time is responsible for improvement in bonding, an effect of the matrix contracting around the fibers. If this is true, then an increase in bond strength, together with a decrease in fiber debond length would result in a fall in toughness of the composite. The measured work of fracture of glass fibers in epoxy is 280 kJ/m^2, approximately, and 200 kJ/m^2 after storing for 6 months. Table III shows the predicted energy terms calculated using the models of fracture, together with average values of debond length and pull-out length of the glass fibers used in the calculation. In the mechanism involving debonding and slippage, aging has approximately halved the value of the post-debond fiber sliding parameter. The agreement between theoretical energy and experimental work of fracture is a good one.

Glass fibers and carbon fibers in epoxy

Fractographic information of glass fibers in a hybrid composite is summarized in the following cumulative probability diagrams (Figs. 18-20). The fiber debond length data do not superimpose, and increasing the ratio of glass fibers to carbon fibers may displace the data to the right or to the left of the diagram (Fig. 18). For example, increasing the glass fiber content from 30 % (by vol.) to 56 % (by vol.) of the total fiber content shifts the data from low values of fiber debond length to high values of fiber debond length; increasing the glass fiber content by a further 7 % (by vol.) moves the data back to lower values. Closer examination of the data shows the subtle effects of composition on the position of the cumulative probability curve. These effects will be referred to later.

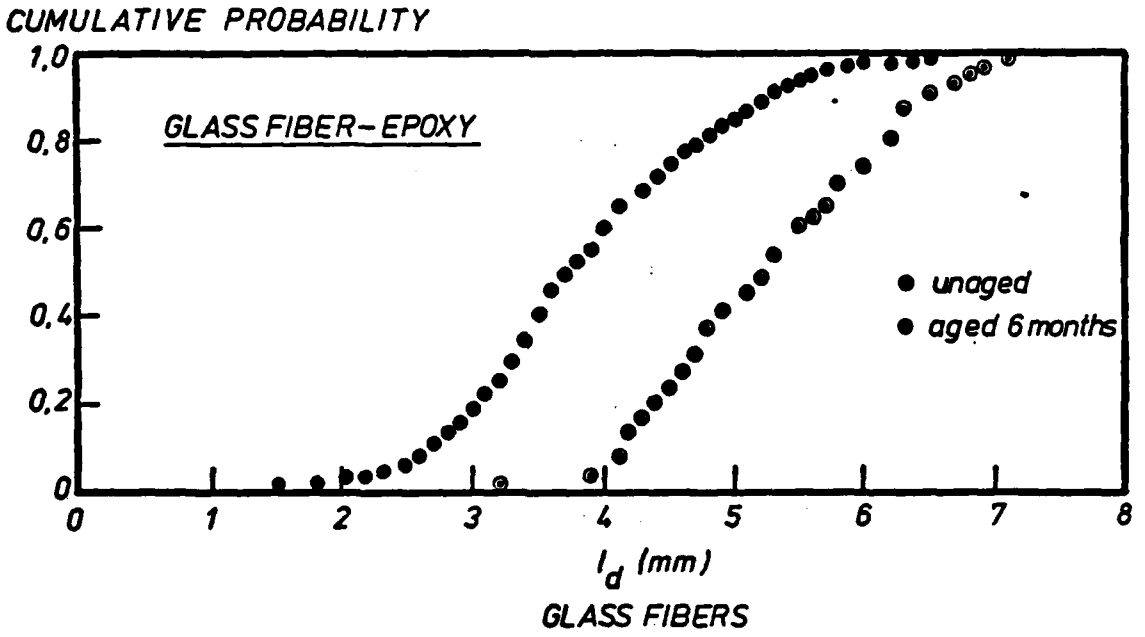

Fig. 16. Extreme value distributions of lengths of debonded glass fibers in epoxy before and after aging for 6 months at 18 (± 2) °C, 65 % R.H.

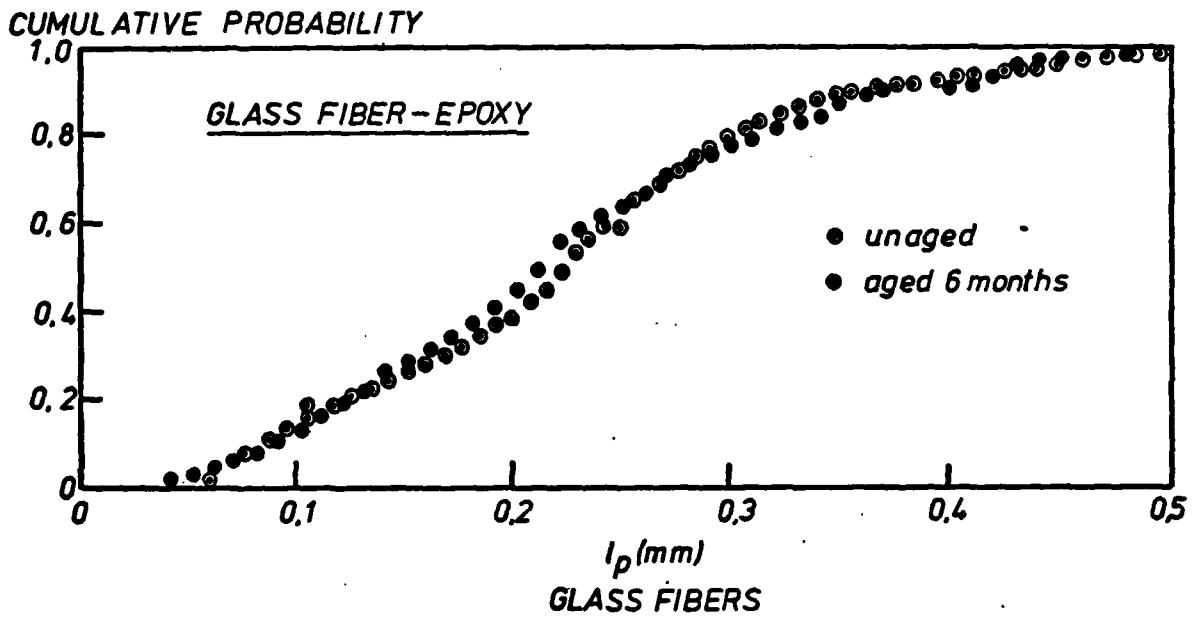

Fig. 17 Extreme value distributions of lengths of pulled out glass fibres in epoxy before and after aging for 6 months at 18 (± 2) °C, 65 % R.H.

TABLE III

Effect of aging for 6 months upon the fracture energy of a glass fiber-epoxy composite

	W_{pdf}	W_d	W_p	W_T	W_{EXPT}
			(kJ/m^2)		
Before aging	226	46	56	272	280
After aging	117	34	58	209	202

These predictions are based on the following measurements:

$\bar{\ell}_d$ (unaged) = 5.3 mm

$\bar{\ell}_d$ (aged) = 3.9 mm

$\bar{\ell}_p$ = 0.24 mm approximately, before and after aging

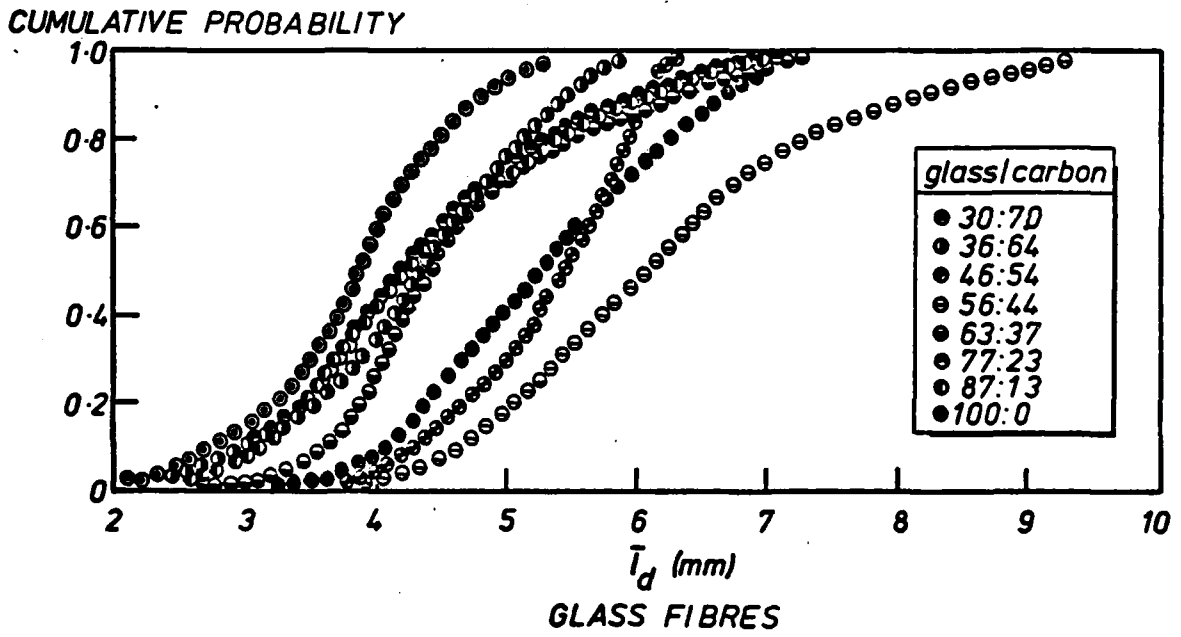

Fig. 18 Extreme value distributions of lengths of debonded glass fibers in hybrid composites (epoxy matrix).

In contrast, data of glass fiber pull-out length in the hybrid composite are almost superimposed (Fig. 19). The same applies to the data for carbon fibers (Fig. 20). Each cumulative probability curve overlaps with one another and the shape and position of the curves are not significantly affected by variations in composition. The same data plotted, in a logarithmic form based on eq. (11), is used to determine values of m and l_o (see eq.(15)(Table IV). Taking average values of fiber debond length and fiber pull-out length for the glass fibers and carbon fibers, combined with the equations of fracture energy, we can estimate the energy dissipated during fracture and pull-out of both kinds of fiber. In this case, fracture energy is plotted against percentage of carbon fibers in the hybrid composite (Figs. 21-26).

Figure 21 shows an estimation of the energy dissipated during glass fiber-matrix sliding soon after the bond has failed. While there is an overall decrease in energy as the carbon fiber content increases, as one would expect, it by no means forms a linear relationship. Certain features are worth pointing out. The first is that after a sharp drop in energy as glass fiber is replaced with carbon fiber, a plateau is observed up to 40 % (by vol.) of carbon fiber. At that point, the fracture energy actually increases slightly before falling to zero as the remaining glass fibers are replaced with carbon fibers. Recalling the cumulative probability data, we realize that it is the effects of composition on glass fiber debond length and the subtle balance between debond length and number of fibers which is the origin of the unexpected shape of the post-debond sliding energy diagram. The small peak in the diagram at 44% (by vol.) of carbon fiber coincides with the large displacement of the cumulative probability data to higher values of glass fiber debond length.

At first sight, glass fiber debond energy decreases linearly with an increase in volume fraction of carbon fiber (Fig. 22). Closer inspection shows a shallow curve with a very small peak at 44 % (by vol.) of carbon fiber. Minor differences in shape and position of the cumulative probability curves are responsible for the non-linear behaviour.

Slight undulations in the pull-out curve for the glass fibers can also be identified with minor changes in shape and position of the cumulative probability curves (Fig. 23). As a first approximation, the glass fiber

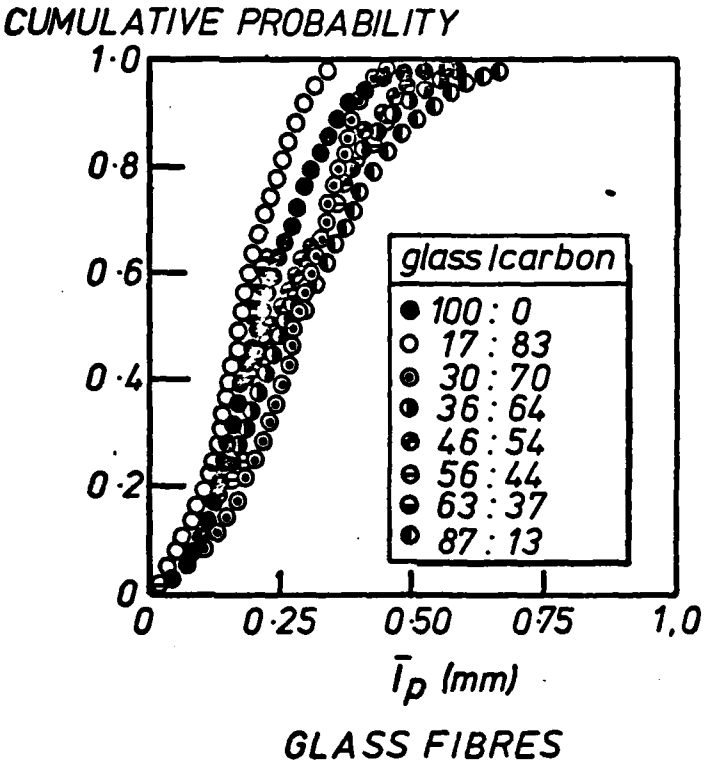

Fig. 19 Extreme value distributions of lengths of pulled out glass fibers in hybrid composites (epoxy matrix).

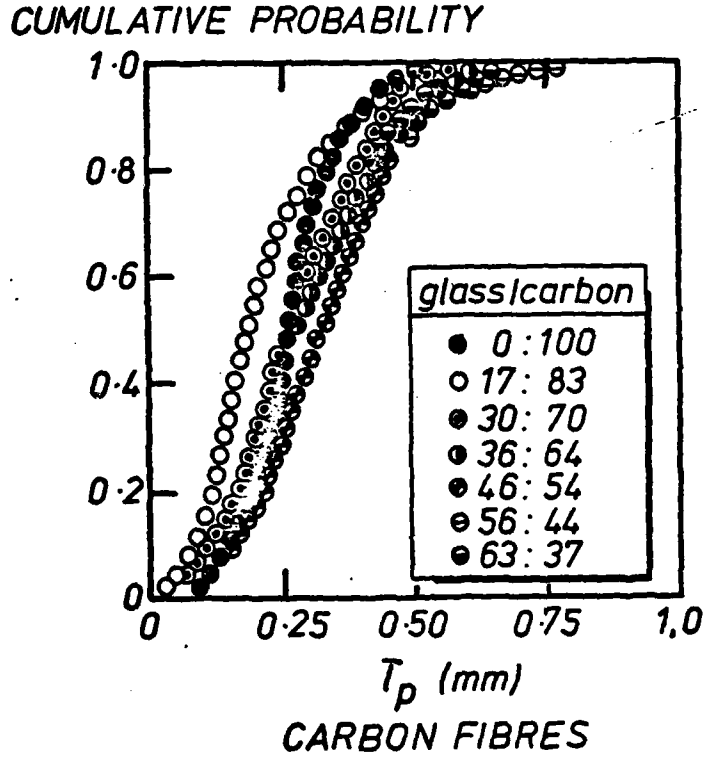

Fig. 20 Extreme value distributions of lengths of pulled out carbon fibers in hybrid composites (epoxy matrix).

TABLE IV

Values of m, ℓ_o, and $\bar{\ell}$ for glass fibers and carbon fibers in epoxy resin

Ratio of C/G	Glass fibers debonding (mm)			Glass fibers pulling out (mm)			Carbon fibers pulling out (mm)		
	m	ℓ_o	$\bar{\ell}$	m	ℓ_o	$\bar{\ell}$	m	ℓ_o	$\bar{\ell}$
0:100	6.9	5.6	5.3	2.4	0.26	0.23	-	-	-
13:87	4.5	4.9	4.4	2.0	0.36	0.25	1.3	0.35	0.32
23:77	4.2	4.9	4.4	2.1	0.24	0.22	2.0	0.31	0.28
37:63	5.3	5.1	4.7	1.6	0.24	0.23	2.0	0.37	0.32
44:56	5.8	6.7	5.9	1.8	0.32	0.27	2.4	0.30	0.33
54:46	9.1	5.6	5.3	1.7	0.30	0.26	2.6	0.39	0.34
64:36	4.8	4.7	4.3	1.9	0.31	0.27	2.2	0.34	0.31
70:30	5.0	4.1	3.8	2.2	0.31	0.28	2.2	0.32	0.28
83:17			2.3	3.4	0.21	0.19	2.2	0.25	0.22
100:0	-	-	-	-	-	-	2.4	0.31	0.28

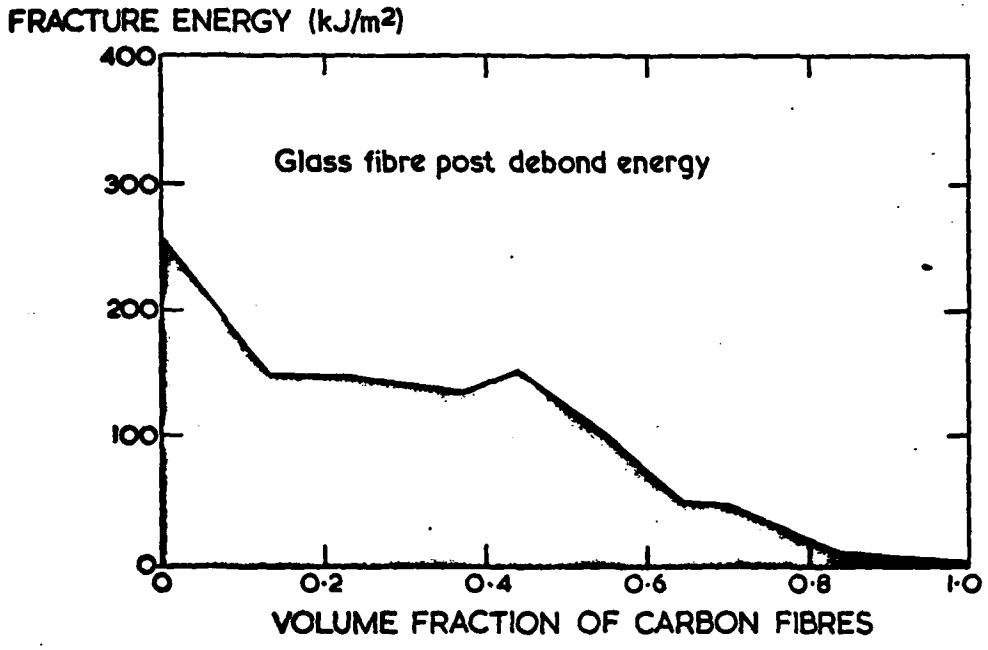

Fig. 21 An estimation of the energy dissipated when a glass fiber debonds and slides in its matrix socket in a hybrid composite system (epoxy matrix).

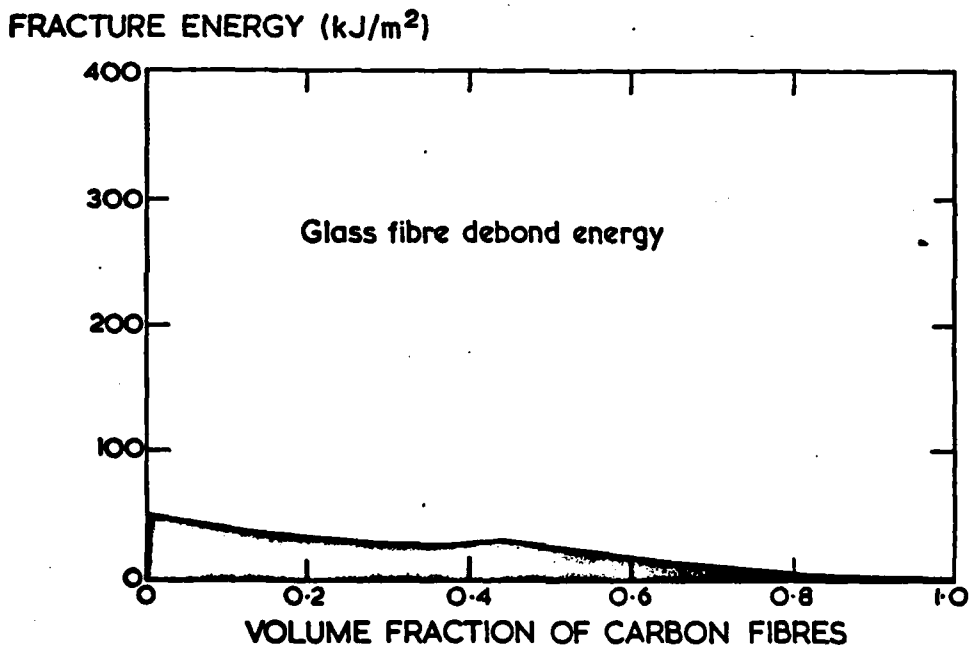

Fig. 22 An estimation of the release of stored elastic strain energy when a debonded glass fiber snaps in a hybrid composite system (epoxy matrix).

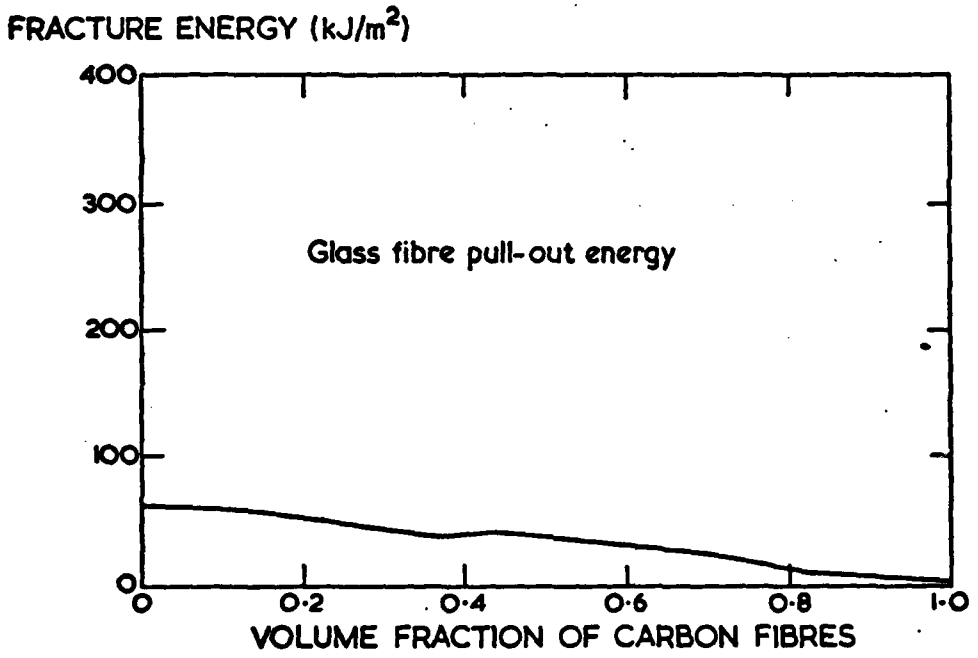

Fig. 23 An estimation of the work done in pulling a broken glass fiber out of a cracked matrix in a hybrid composite system (epoxy matrix).

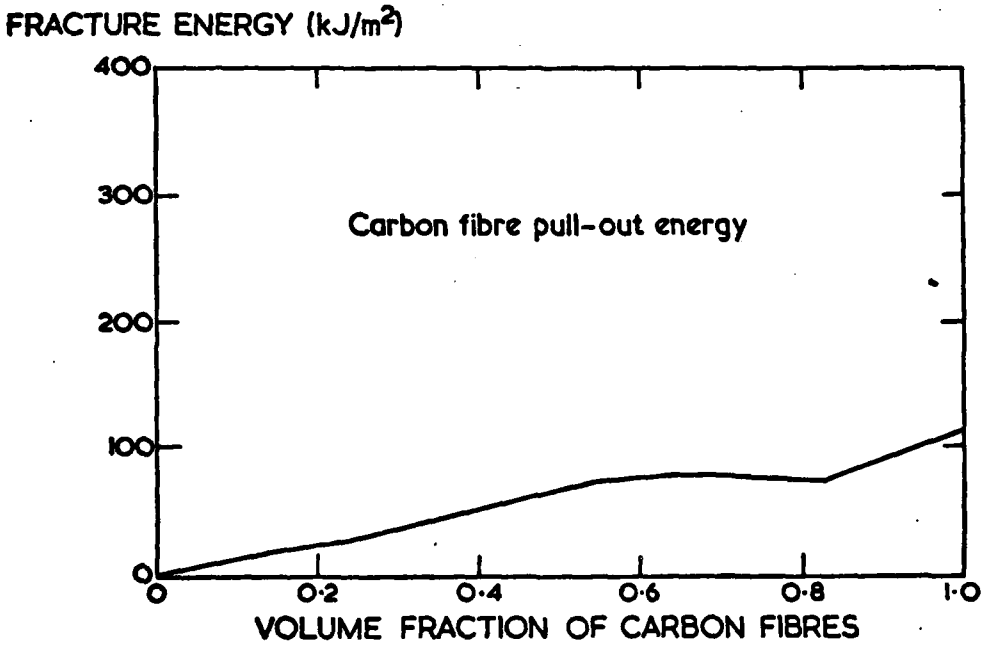

Fig. 24 An estimation of the work done in pulling a broken carbon fiber out of a cracked matrix in a hybrid composite system (epoxy matrix).

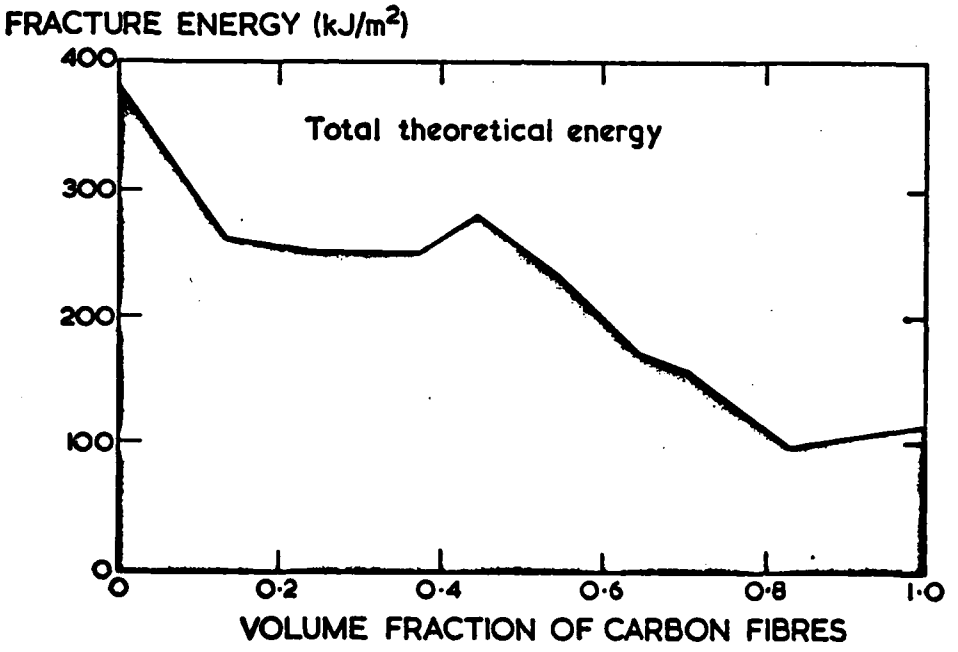

Fig, 25 Total theoretical fracture energy of a hybrid composite system determined from data of debonded length and pull-out length of glass fibers and carbon fibers in epoxy, together with eq. (15).

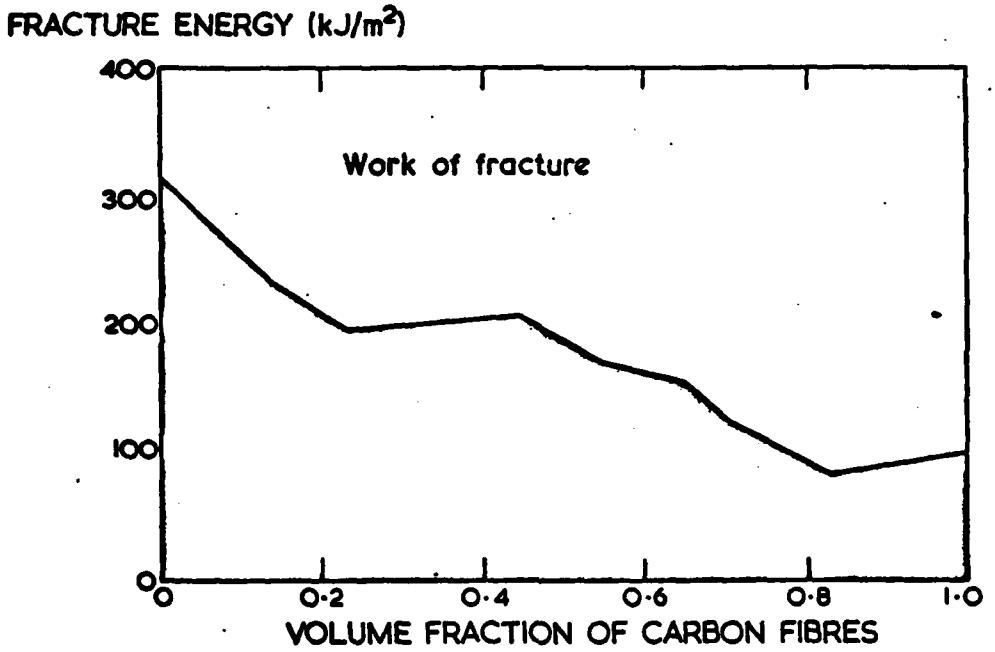

Fig. 26 Experimental work of fracture of a hybrid composite system (glass fibers and carbon fibers in epoxy).

debond energy and glass fiber pull-out energy are directly proportional to the amount of glass fiber in the composite, as one would expect from the form of the equations.

Similar undulations in the carbon fiber pull-out energy diagram originate in the small differences to be found in the cumulative probability data (Fig. 24). Ignoring these minor effects, the pull-out energy follows a linear relationship with carbon fiber content, as one would expect. Figs. 25, 26 show good agreement between theory and experiment.

Glass fibers and carbon fibers in polyester

In this section, we present work of fracture data of a hybrid system with a polyester matrix. Cumulative probability diagrams showing extreme value distributions of fiber debond lengths and fiber pull-out lengths have been constructed and replotted in logarithmic form in order to determine the parameters m and ℓ_o. Data of mean fiber debond length and mean fiber pull-out length, together with the models of micromechanisms of fracture are used to estimate the energies dissipated during crack propagation. Where possible, comparisons are made between the fracture behaviour of the two hybrid systems investigated and the effect of matrix becomes apparent.

Figure 27 shows the experimental work of fracture data for the two hybrid systems. Certain features of the curves are apparent. First, the general shape of the curves are similar and second, the polyester hybrid composites have work of fracture values which are about 50 % higher than values obtained for the epoxy composites. One noticeable exception is the datum point for the glass fiber-polyester; in this case, the work of fracture is less than the value obtained for the epoxy composite. Reference to this apparent anomaly will be made when the distribution of glass fiber debond lengths is discussed.

Figure 28 shows the distribution of glass fiber debond lengths as a function of the composition of the hybrid. As we observed and reported earlier, the position of the extreme value distribution depends upon the ratio of carbon fibers to glass fibers. Closer examination of the two diagrams (Figs. 18 and 28) reveals that the relationship between extreme value distribution and composition is not clear; the movement of cumulative probability curves as the ratio changes is not consistent from one hybrid system to the other. In the case of glass fibers in epoxy, (without carbon fibers), the data are on the extreme right of the diagram, while for the polyester composite, the data are towards the extreme

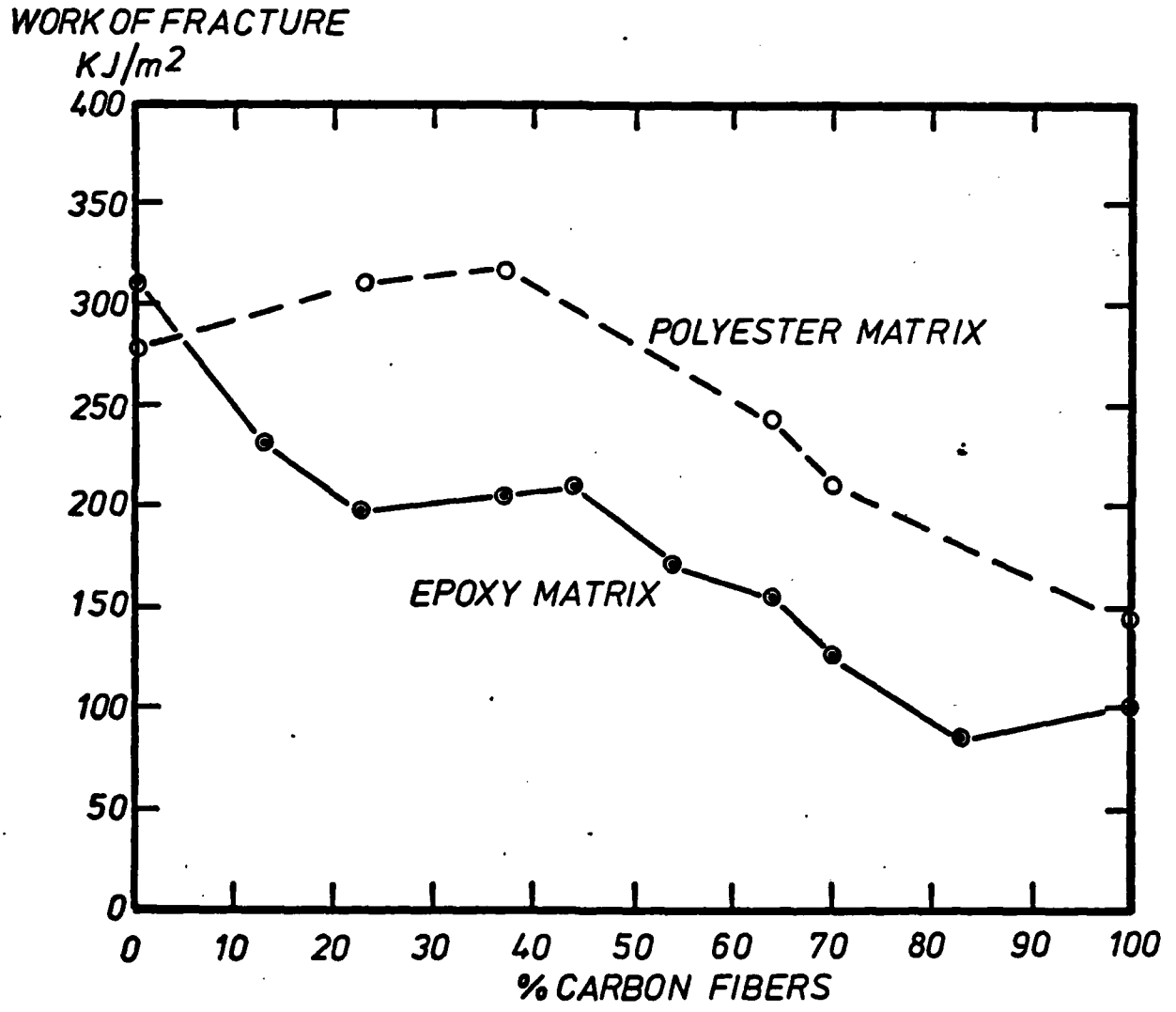

Fig. 27 Comparison between experimental work of fracture data of polyester and epoxy hybrid composite systems.

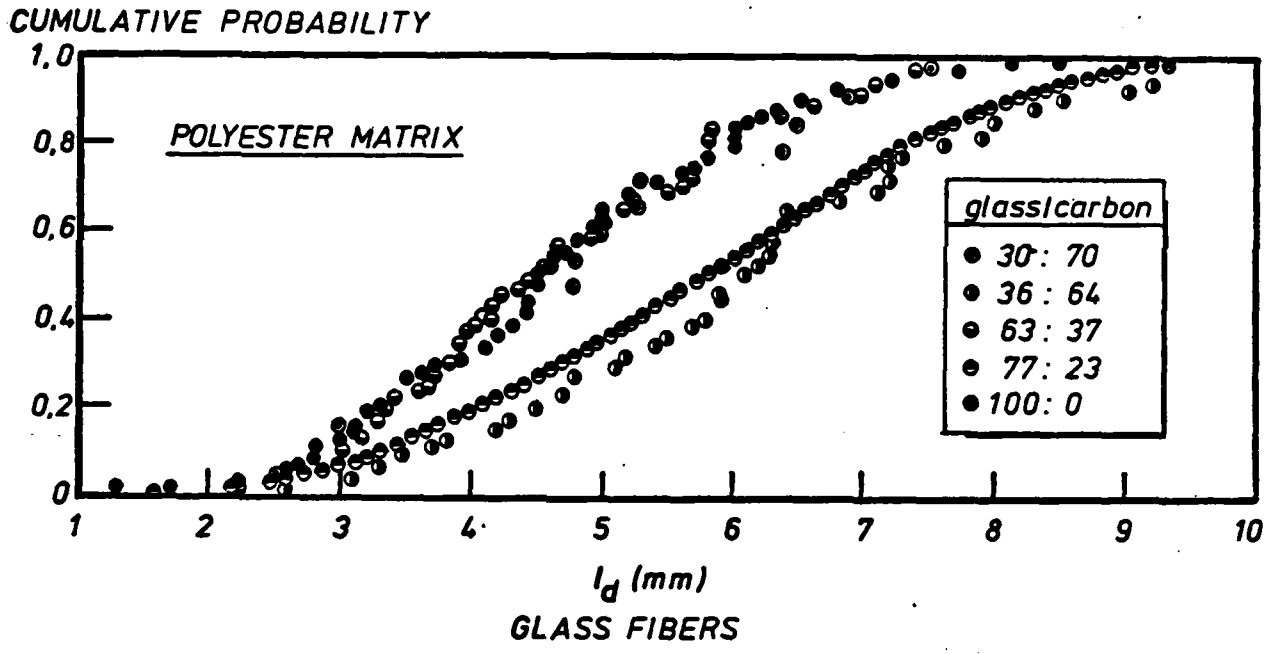

Fig. 28 Extreme value distributions of debonded lengths of glass fibers in hybrid composites (polyester matrix).

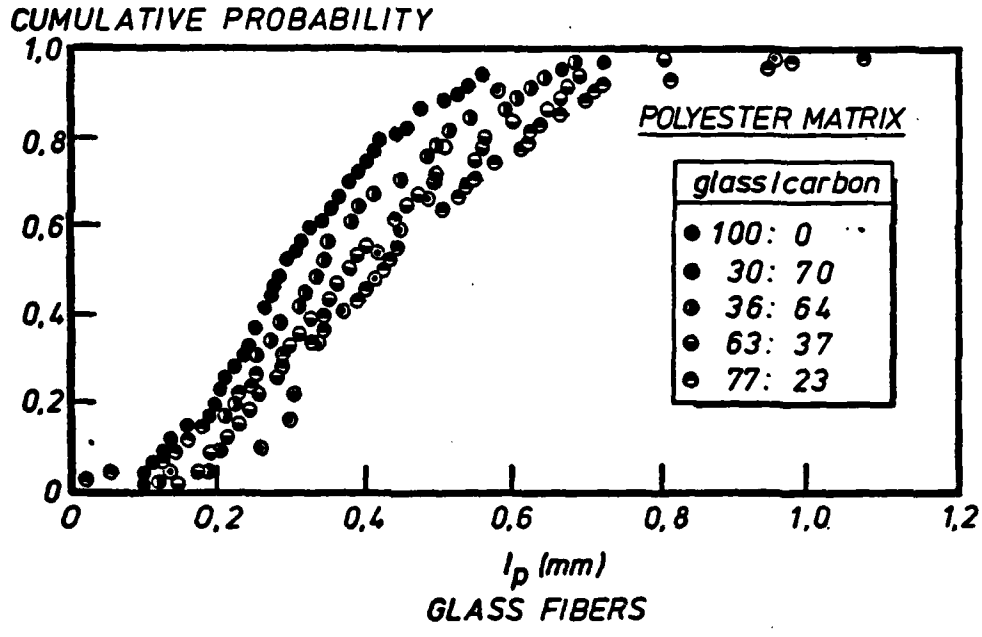

Fig. 29 Extreme value distributions of pulled out lengths of glass fibers in hybrid composites (polyester matrix).

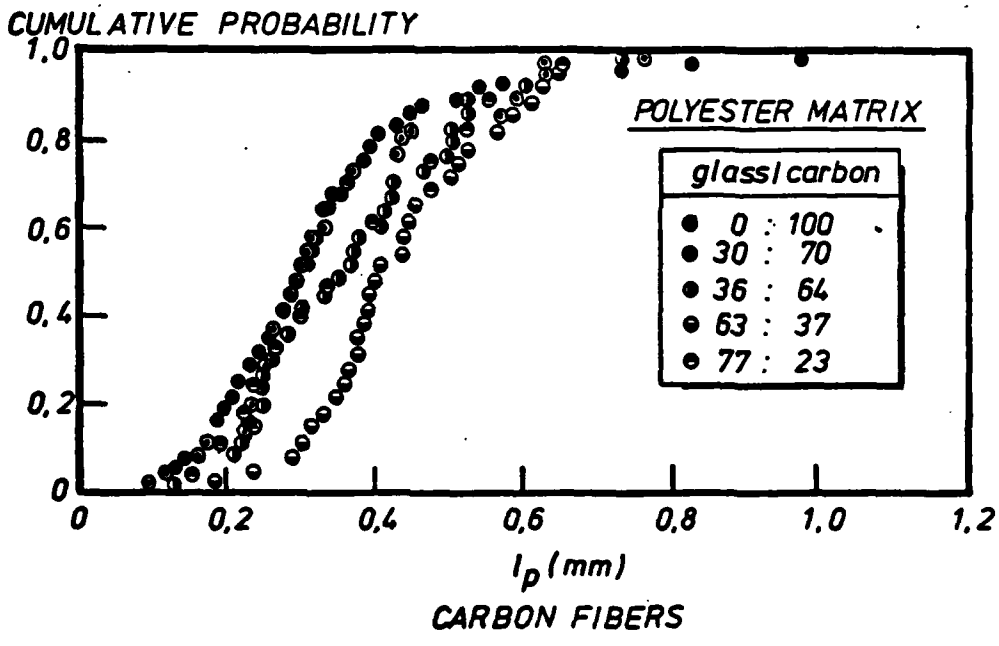

Fig. 30 Extreme value distribution of pulled out lengths of carbon fibres in hybrid composites (polyester matrix).

left. It is the apparently low value of debonded lengths of glass fiber in polyester that we believe is responsible for the low work of fracture measurement to which reference was made earlier.

Values of m, ℓ_o and $\bar{\ell}$ for the polyester hybrid composites are listed in Table V. In the case of the debonding of glass fibers, m values are slightly higher for epoxy than polyester, while ℓ_o values are essentially independent of the choice of matrix.

For the extraction of broken glass fibers from their matrix sockets, values of m are similar for the two resins, while ℓ_o values are slightly higher for the polyester. In the pulling out of carbon fibers, values of m and ℓ_o are less for the epoxy than polyester. The indication is that the interfacial bond strength between fiber and matrix is greater for the epoxy composite and the toughness is correspondingly lower. A similar observation was made a few years ago by Beaumont and Harris (7).

Average values of debond length and pull-out length for glass fibers and carbon fibers, given in Table V, were used, together with the models of fracture to predict energies of post-debond fiber sliding, fiber debonding (elastic deformational energy), and fiber pull-out. Estimations of these energy parameters for glass fibers and carbon fibers are shown in Figures 31-36. Certain comments can be made and generalisations drawn from comparison of the fracture energy diagrams (Figs. 27, 28, 35, 36). The overall shapes of the theoretical and experimental fracture energy curves are similar; and the relative order of magnitudes of the four energy parameters and the contribution each one makes to the total fracture energy or toughness of the composite are also alike. The shape of both total theoretical fracture energy curves is dominated by the post-debond fiber sliding term for glass fibers; and at the carbon fiber-rich end of the diagram, the pull-out term for carbon fibers is important. Comparison between the theoretical fracture energy and experimental work of fracture data show remarkable similarities in shape and magnitude. For glass fibers, the post-debond sliding energy term is a major component of the total fracture energy, while the debonding energy and pull-out energy terms are comparable in magnitude. Together, debonding and pull-out of glass fibers contribute no more than one-quarter of the total fracture energy of the hybrid composite. On the other hand, carbon fibers were not observed to debond, and the work done in extracting them from a cracked matrix can be successfully equated to the fracture energy of a carbon fiber composite.

TABLE V

Values of m, ℓ_o, and $\bar{\ell}$ for carbon fibers and glass fibers in polyester

Ratio of C/G	Glass fibers debonding (mm)			Glass fibers pulling out (mm)			Carbon fibers pulling out (mm)		
	m	ℓ_o	$\bar{\ell}$	m	ℓ_o	$\bar{\ell}$	m	ℓ_o	$\bar{\ell}$
0:100	3.6	5.2	4.7	2.5	0.35	0.31	-	-	-
23:77	3.4	6.6	5.8	2.0	0.53	0.45	2.7	0.42	0.37
37:63	4.1	5.1	4.7	2.7	0.46	0.41	4.2	0.48	0.44
64:36	4.0	6.7	6.0	2.8	0.41	0.37	3.0	0.42	0.37
70:30	3.7	5.3	4.7	2.5	0.49	0.43	2.6	0.38	0.34
100:0	-	-	-	-	-	-	2.7	0.37	0.33

Work of fracture of structural fibrous composites

Model specimens of the kind used in this study can be used to estimate the work of fracture of structural fibrous composites. Consider, for example, a structural unidirectional glass fiber or carbon fiber composite, fabricated to the dimensions of the model composite, 20 mm x 10 mm x 2 mm. If the fiber volume fraction is 0.5, then the total cross-sectional area of the fibers is 10×10^{-6} m^2. In a model composite containing 5 tows of carbon fiber, for instance, the total cross-sectional area of the fibers is 1.4×10^{-6} m^2, approximately. There are about 7 times as many fibers in the structural composite compared to the model composite. If we multiply the measured fracture energy of the model carbon fiber composite by 7 times, and in the case of the model glass fiber composite containing 5 strands by 8.5 times, we can estimate the work done in breaking the structural composite. The work of fracture of the structural composite is calculated by simply dividing the estimated work to break the specimen by twice its cross-sectional area. Table VI lists the work of fracture of several carbon fiber and glass fiber structural composites estimated in this way. They are based on measurements of work of fracture obtained using the model composite specimens. These values are very close to measurements made by others using fracture mechanics specimens, (see, for example, Harris and Bunsell (8) and Beaumont and Phillips (9), but in those cases, a detailed failure analysis was not carried out and would have been extremely difficult to have done so.

CONCLUSIONS AND IMPLICATIONS

When a crack passes through a hybrid composite, the glass fibers are observed to debond and together with the carbon fibers fracture, pulling out of the resin as the surfaces of the matrix crack open. Models based on these observations, predict the energies dissipated when a debonded fibers slides in its socket, snaps and pulls out of the matrix. Detailed comparisons of experimental data combined with the models show that the post-debond fiber sliding mechanism is primarily responsible for the work to fracture glass fibers in epoxy or polyester matrices, while the fiber pull-out mechanism accounts for the fracture energy of carbon fibers in epoxy or polyester resins. It is the subtle balance between these mechanisms and the volume fraction of the carbon fibers and glass fibers in the hybrid composite, and the effects of composition upon the mechanisms of debonding and pull-out where lies the origins of toughness of the hybrid fiber systems.

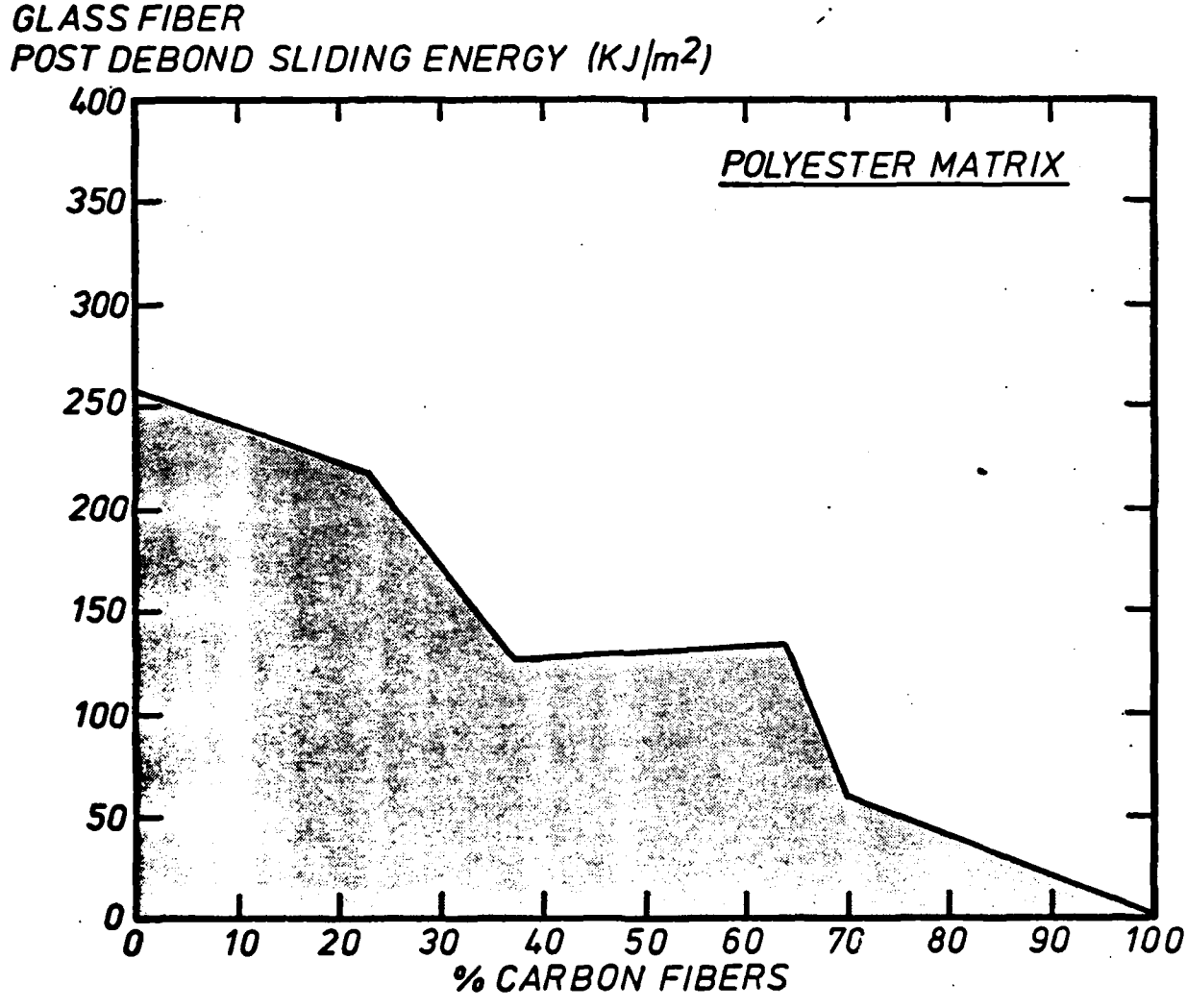

Fig. 31 Estimation of the energy dissipated when a glass fiber debonds and slides in its matrix socket in a hybrid composite system (polyester matrix).

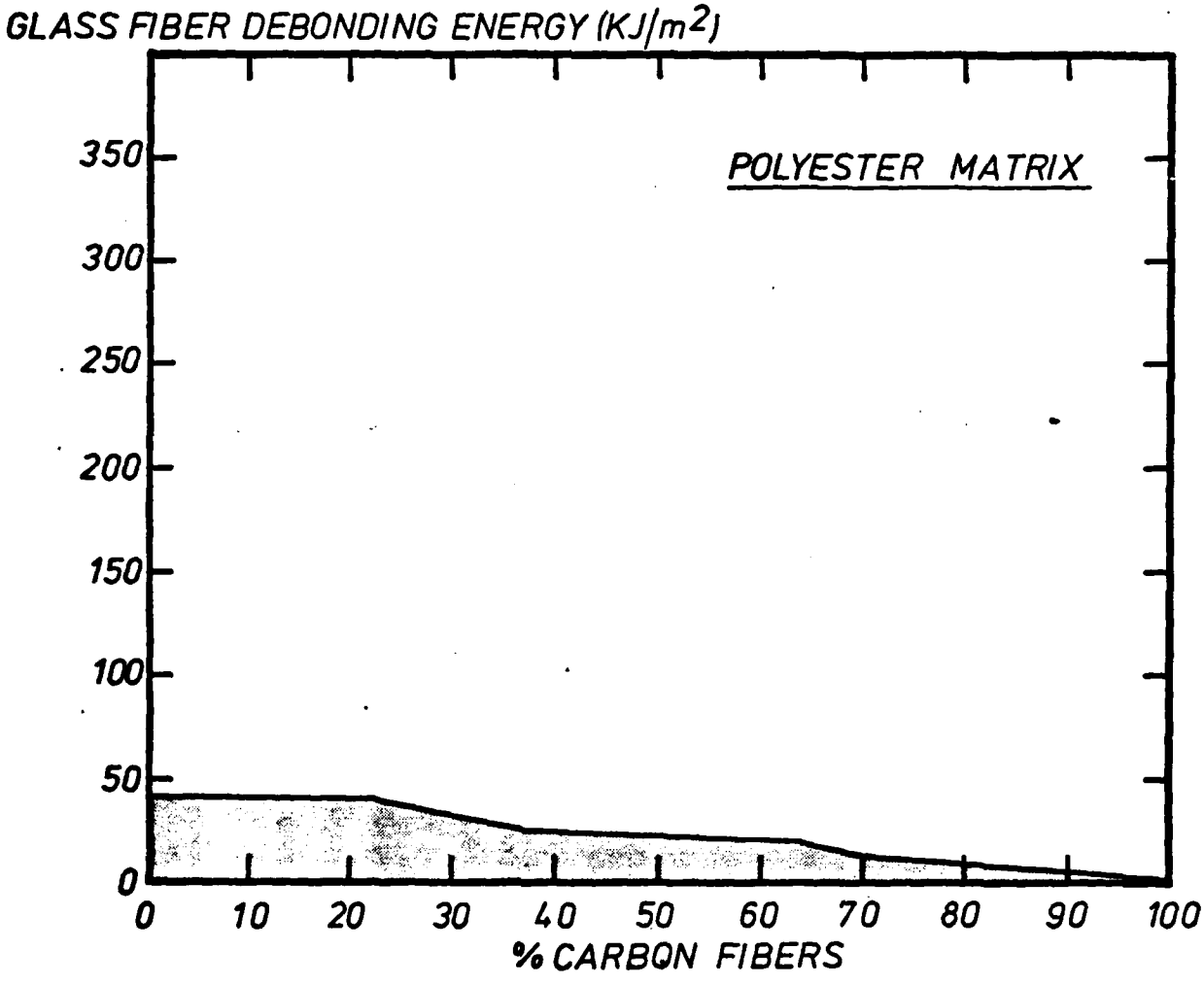

Fig. 32 Estimation of the release of stored elastic strain energy when a debonded glass fiber snaps in a hybrid composite system (polyester matrix).

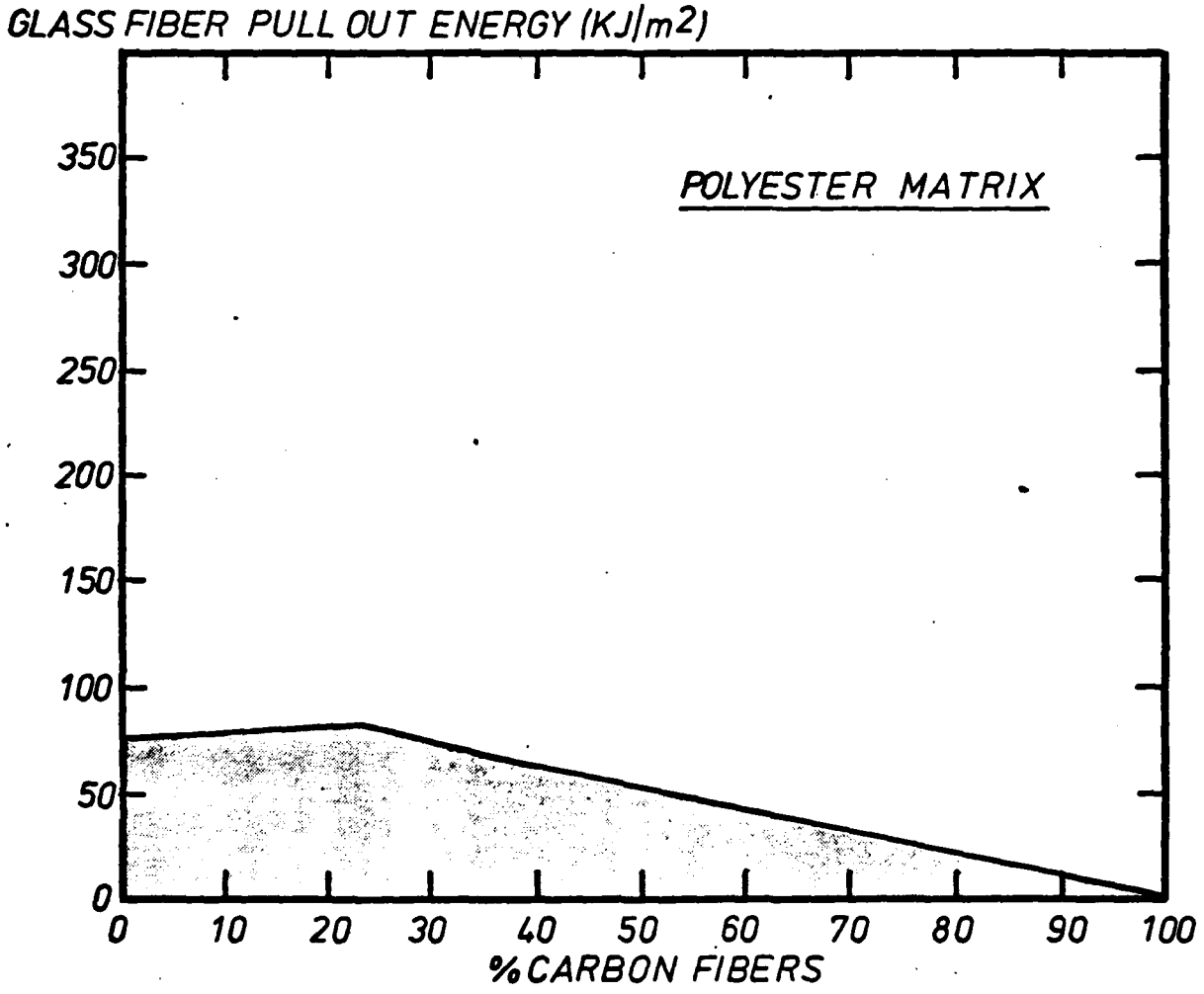

Fig. 33 Estimation of the work done in pulling a broken glass fiber out of its matrix socket in a hybrid composite system (polyester matrix).

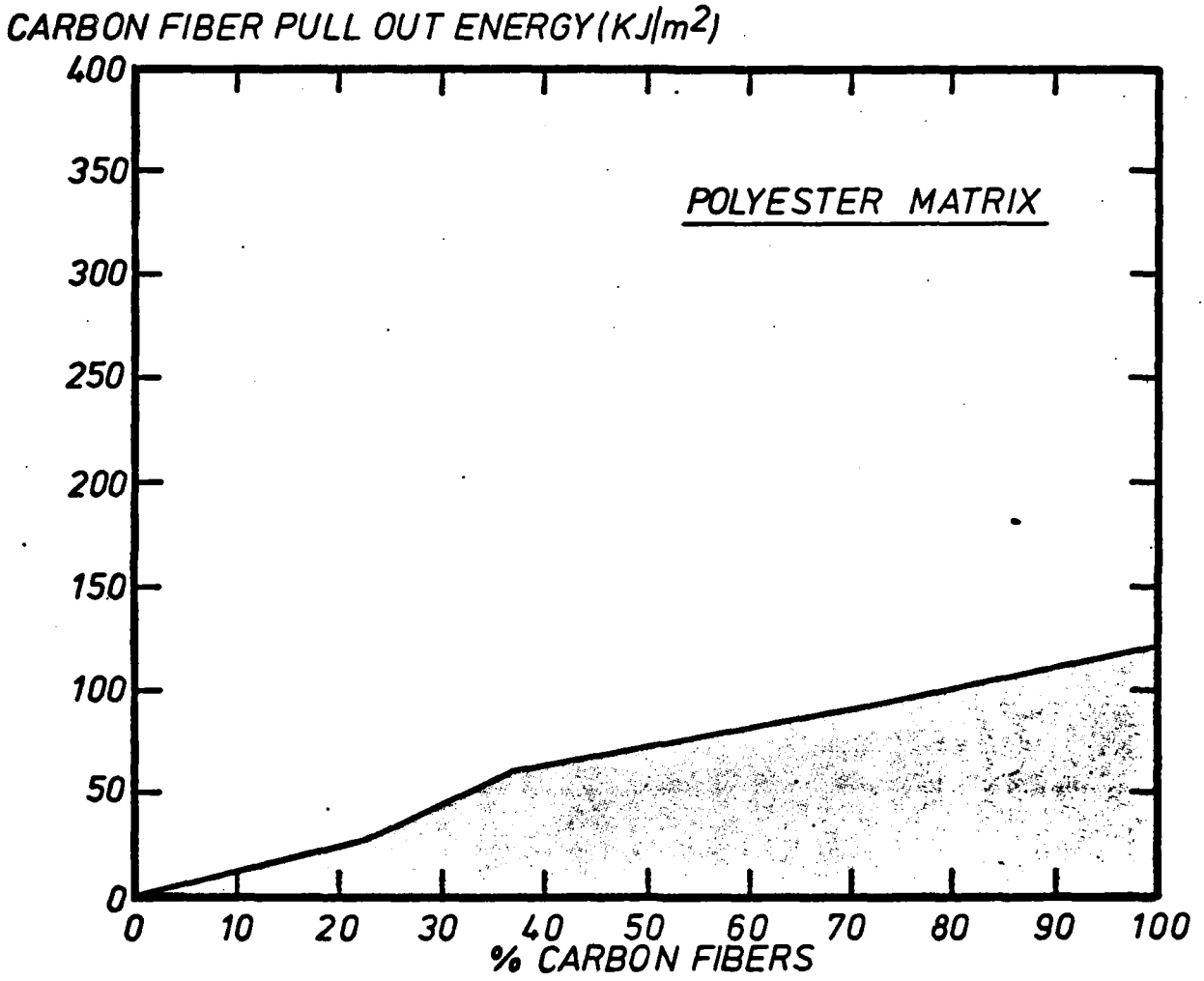

Fig. 34 Estimation of the work done in pulling a broken carbon fiber out of its matrix socket in a hybrid composite system (polyester matrix).

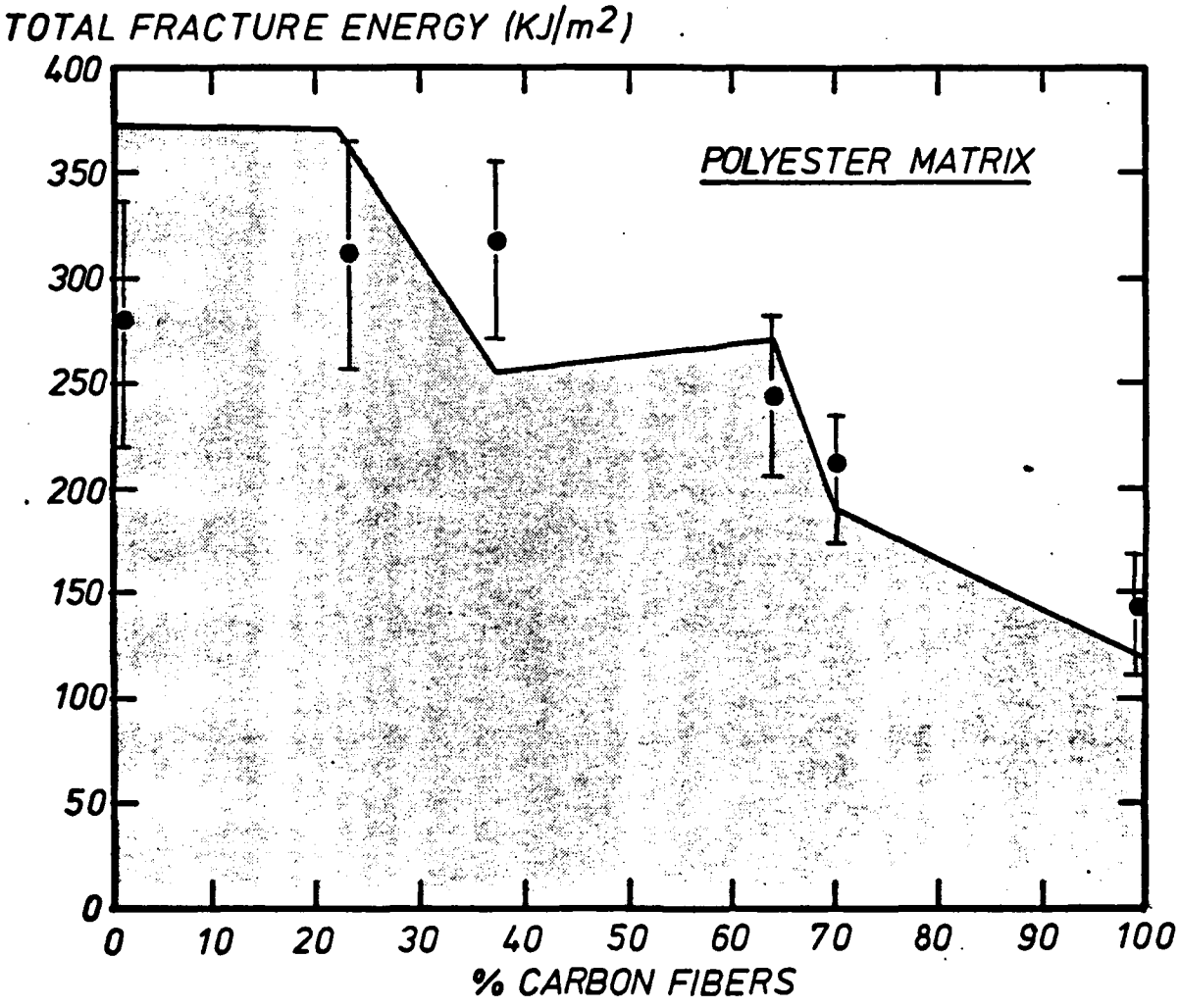

Fig. 35 Total theoretical fracture energy of a hybrid composite system (carbon and glass fibers in polyester). The points represent measured work of fracture data.

TABLE VI

Material	Work of fracture (kJ/m^2)
Carbon fiber/epoxy	48
64%Carbon fiber/36%glass fiber/epoxy	75
Glass fiber/epoxy	148
Carbon fiber/polyester	70
64%Carbon fiber/36%glass fiber/polyester	118
Glass fiber/polyester	132

(The nominal fiber volume fraction is 0.5)

ACKNOWLEDGEMENTS

We wish to acknowledge the support of the Air Force Office of Scientific Research, Washington, D. C., under grant number AFOSR-78-3644.

REFERENCES

1. A. Kelly, Proc. Roy. Soc. A319, 95, (1970).

2. B. Harris, J. Morley and D. C. Phillips, J. Mater. Sci. 10, 2050 (1975).

3. J. O. Outwater and M. C. Murphy, Modern Plastics 7, 160, (1970); see also J. Adhesion 2, 242, (1970).

4. M. R. Piggott, J. Mater. Sci. 5, 669 (1970).

5. J. FitzRandolph, D. C. Phillips, P. W. R. Beaumont and A. S. Tetelman, J. Mater. Sci. 7, 289, (1972).

6. A. H. Cottrell, Proc. Roy. Soc. A282, 2, (1964).

7. P. W. R. Beaumont and B. Harris, J. Mater. Sci., 7 (1972) 1265.

8. B. Harris and A. R. Bunsell, Composites, 6, (1975), 197.

9. P. W. R. Beaumont and D. C. Phillips, J. Composite Materials, 6 (1972) January.